JOURNAL OF MATERIALS SCIENCE **33** (1998) 5535–5556

Mesoscopic aspects of polymer composites: Processing, structure and properties

K. FRIEDRICH
Institut für Verbundwerkstoffe (IVW), University of Kaiserslautern, 67663 Kaiserslautern, Germany

There can be little doubt that the morphology of the polymer matrix, the geometrical arrangement of the reinforcing elements and the existance of flaws, all on a mesoscopic scale between a few micrometers to several millimeters, have a strong influence on the performance of composite materials. Mesomechanics describes the properties of these mesostructures. Most of the latter are a result of the particular processing conditions used for the various types of composites. This is demonstrated (in form of examples of the author's own experience) for an unfilled semicrystalline polypropylene, a blend of epoxy resin with an elastomeric toughener, an injection moldable short fiber reinforced polyethyleneterephthalate, a discontinuous aligned fiber/polyethersulfone composite, and a high performance continuous fiber reinforced polymer composite system respectively. Mesostructural design is discussed with regard to some possibilities of how to optimize the various mesostructures of these materials, in order to achieve a particular property profile.

1. Introduction and definitions

The science and technology of fiber composites are established upon a design concept that is markedly different from that of conventional structural materials [1]. Due to the fibrous nature of the reinforcing phase, composite materials offer the opportunity to tailor material characteristics so as to match performance requirements. In addition to the selection of reinforcing fibers and matrix material, tailoring in continuous fiber systems is accomplished through the control of reinforcing geometry during the manufacturing process. The final structure may be deliberately constructed by laminations of collimated fibers or the selection of various woven or braided architectures [2].

In case of discontinuous ("short") fiber reinforced composites the resulting structure of the material is even more dependent upon processing conditions and processing history. Variations in fiber orientation and fiber lengths induced during the fabrication of injection molded parts can cause significant variations in the overall mechanical behavior. The richness of possible reinforcing geometries through these various arrangements can give rise to a wide range of properties for composite materials of equivalent composition [2]. For a given macrostructure with properties planned in the original design, there will be a range of actual (lower or better) properties achieved [3]. The reasons for these differences can be found in geometrical and structural imperfections of the material at different levels of magnification. This "structural hierarchy", as defined by Eduljee and McCullough [2], can vary in composite materials from (a) the atomic or molecular structure of the composite components via (b) their microstructures to (c) the arrangement of these components on a macro-composite level. The step from (b) to (c) is, however, quite wide because within this intermediate range there are many structural details which are highly affected by the processing conditions. Therefore, it is wise to extend the "hierarchical model" by an extra term called "mesostructure" ("meso" comes from the Greek "mesos" for middle and has been widely used, e.g. meson, mesozoic, mesomorph, etc.). If one defines the mesostructure as structures on a scale between about 1–30 μm and 1–30 mm, packing irregularities and misalignments due to waviness or other causes can be included. The lower part of the range, i.e. about 1–300 μm, is appropriate for effects of matrix morphology and out-of-plane fiber arrangements. The upper range, 300 μm to 30 mm, is more relevant for in-plane variations. Note that these structures, so far at least, are unintentional [3].

At the low levels of magnification associated with lamination theory, a macroscopic body is subdivided into apparent layers with each layer treated as a homogeneous (but anisotropic) material. The internal structure of the individual layers is ignored; the averaged properties of an individual layer (or lamina) are frequently taken from data of the manufacturer [2]. However, from a mesoscopic point of view, variations in ply thickness, non-symmetry effects and differences in the actual ply orientation (relative to the desired one) can cause deviations from the design properties.

At a higher level of magnification, the heterogeneous nature of the individual layer is revealed. The reinforcing fibers are usually provided in the form of tows (or bundles) or individual filaments; the remnants of this

original structure are frequently manifested as fluctuations in the packing geometry, local fiber orientation, and packing density of the filaments. In addition, local flaws or voids due to poor impregnation during processing can occur. Layered structures are also encountered in injection molded short-fiber/thermoplastic matrix composites. In this case the non-uniform flow fields within the mold cavity establish varying fiber orientations that give rise to "skin-core" layers [2]. All of these are typical mesostructural features, which were systematically classified by Piggott [3] into four categories:

(a) Orientation disorder (incl. fiber waviness);
(b) Packing disorder (voids, matrix and fiber rich regions);
(c) Orientation order (layer structure in injection molded short fiber composites);
(d) Packing order (fiber bundling, end synchronization).

While (a) and (b) primarily refer to continuous fiber reinforced systems, subjects (c) and (d) describe the situations in discontinuous fiber reinforced materials. Details are schematically illustrated in Figs 1 and 2.

At yet a higher level of magnification, the heterogeneous nature of individual fibers and matrix becomes important (microstructure). For example, carbon fibers are heterogeneous materials comprised of rigid crystalline graphitic inclusions embedded in an amorphous carbon matrix; organic aramid fibers are similary comprised of rigid crystalline and compliant amorphous components. Semi-crystalline thermoplastic polymer matrices are comprised of various "spherulitic", "lamellar", and "fibrillar" crystalline morphologies embedded in an amorphous component [2]. A focus on this reduced scale takes also into account inhomogeneities in the internal structure of the reinforcing agents and matrix (e.g. voids), the possibility of perturbed interphase regions near the surface of the reinforcing agents, and the different morphologies that can occur when two polymers are blended (Fig. 3). Attempting to establish a demarcation between mesostructure and microstructure is bound to be unsatisfying. Nonetheless, there can be little doubt that the morphology of the reinforcement, the matrix, and the existence of flaws play major roles in composite material properties, albeit roles that are not completely understood [4].

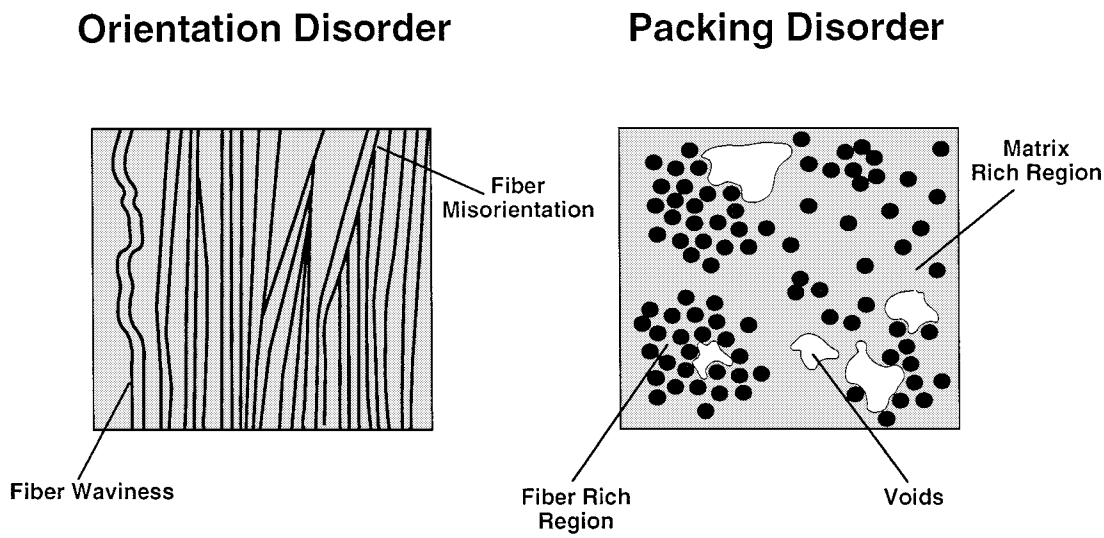

Figure 1 Mesostructural features typical for continuous fiber reinforced composites.

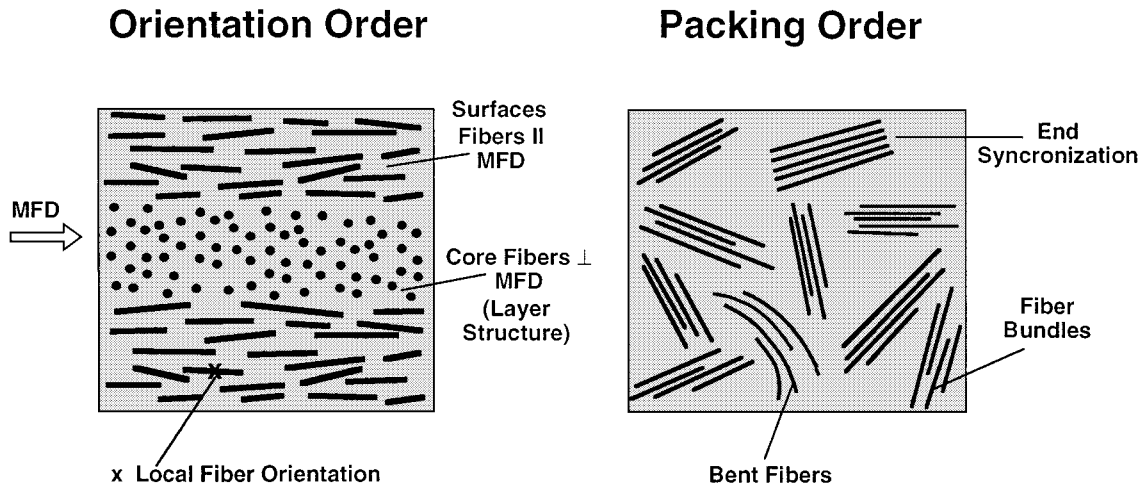

Figure 2 Mesostructural features typical for discontinuous fiber reinforced composites.

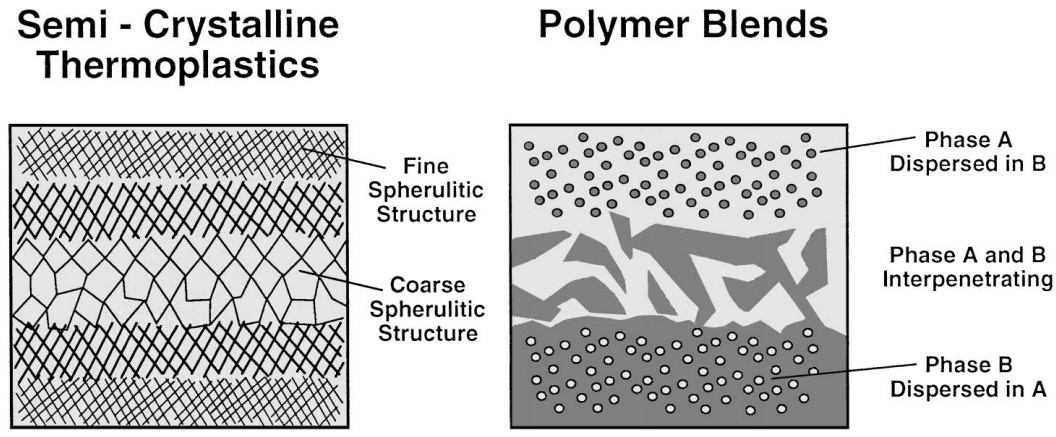

Figure 3 Various morphologies in polymeric materials: Variation in spherulite size across the thickness of injection molded parts (left); possible blend structures as a function of composition between phase A and B.

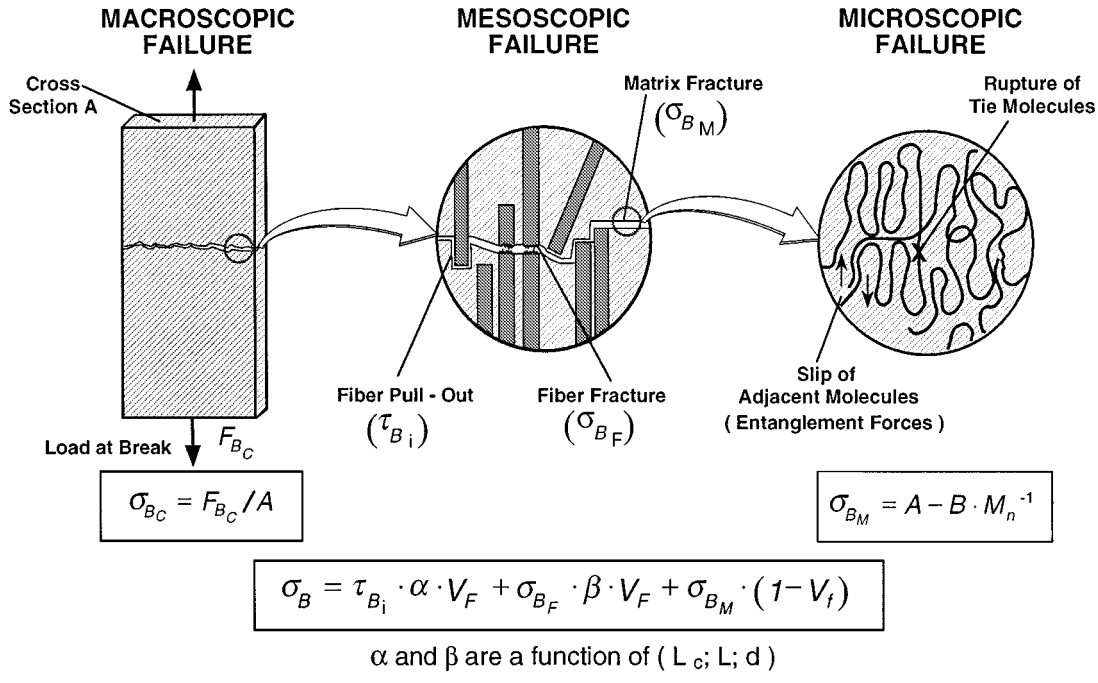

Figure 4 Levels of failure in a short fiber reinforced thermoplastic matrix system.

The next lower level of organization is envisioned as a network system. The nodal points of the network are associated with chemical crosslinks, physical entanglements, and/or regions of localized order stabilized by intermolecular interactions. The links between nodal points are associated with the flexible character of weakly interacting disordered structures. Further magnification on this molecular level reveals the unit cell structure of the crystalline morphologies and the molecular structure of the amorphous components. It is well accepted that the physical properties of polymeric materials have their own origin in the interactions within and between molecules. Continuum properties such as stiffness, strength, damping, etc. are gross descriptions of response characteristics which are the consequence of the reaction of molecules to external actions such as an external force, a change in temperature, etc. [2].

It is obvious that within the intermediate magnification range the mesostructural details control the properties of the composites. In this respect, the term "mesomechanics" can be used to describe the mechanics of mesostructures. It considers the occurence of discrete features of the structure and their effects on mesostructural failure events (Fig. 4). To improve the properties needs a strong control of processing so as to produce the most beneficial mesostructures. "Mesoscopic materials" can therefore be defined as materials in which a high functional quality was achieved through a systematic control of their structure on a mesoscopic scale [5]. "Mesostructural design" is finally based on a better knowledge of the relationships mentioned above. In this respect, further advances in man-made materials can also be achieved through guidance from nature, i.e. the discipline of biomimetics [6, 7]. A typical example is shown in Fig. 5, illustrating the longitudinally and radially arranged, interwoven cellular composite structure of wood. The long vertically oriented cells help to bring water up the tree and also serve a mechanical role. In addition, a radial structure across the wood surface serves to link the load bearing cells in the vertical direction.

The purpose of the present contribution is to give a set of examples how the processing conditions of various

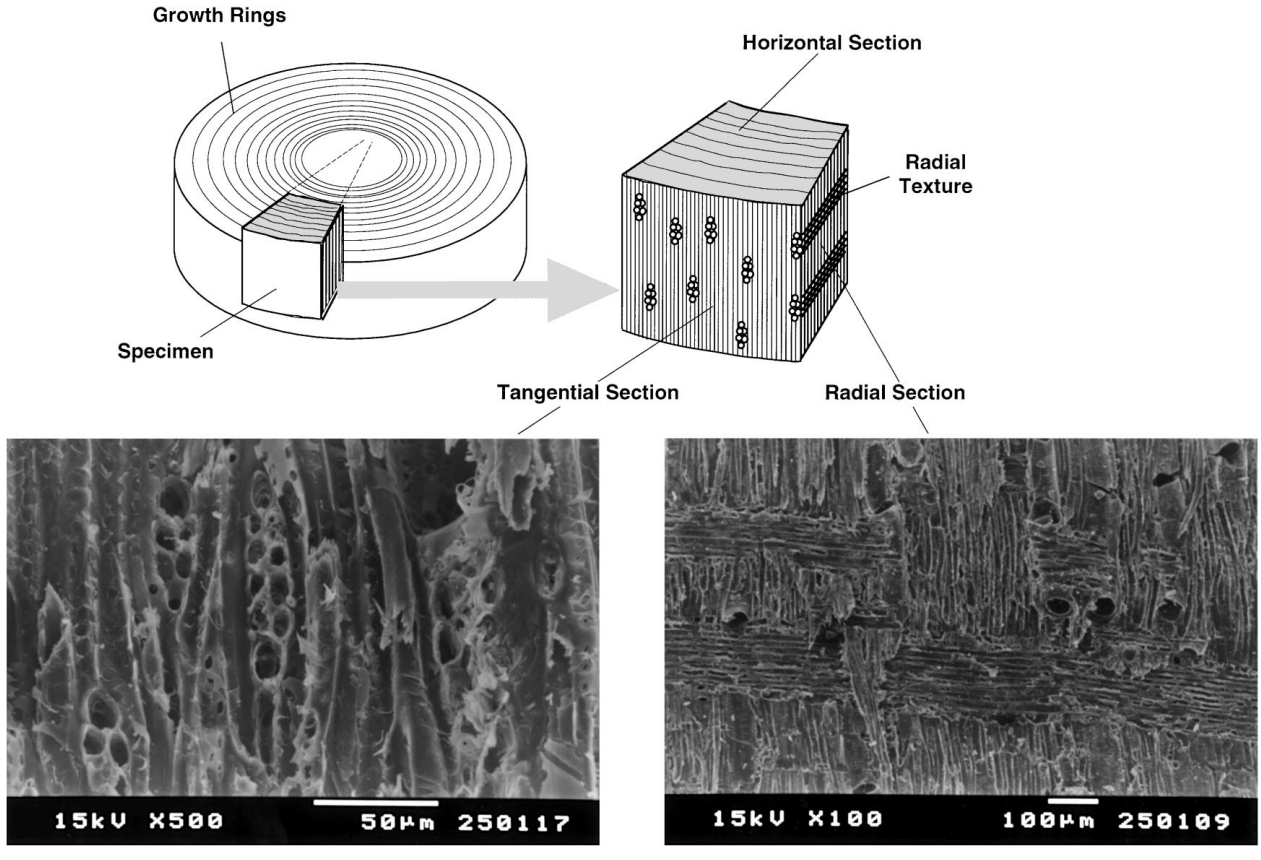

Figure 5 Schematic illustration of wood structure and its scanning electron microscopic evidence (H. Giertzsch, IVW, 1997).

polymer matrix systems affect their mesostructures and the related mechanical properties. Examples include various morphologies in an unfilled semicrystalline polypropylene (PP), a blend of epoxy resin (EP) with an elastomeric toughener, an injection moldable short fiber reinforced polyethyleneterephthalate (PET), a discontinuous aligned fiber, polyethersulfone (PES) composite, and a continuous fiber/high performance composites on the basis of glass fiber (GF)/polypropylene. Many examples of other systems, as they can be found in the scientific literature, would lead to the same conclusions, but as it is not possible to get hold and refer to all of them, the author decided to use only cases of the author's and his group's long years experience in this field.

2. Mesostructural effects on fracture of polypropylene

Deformation and fracture processes influenced by the morphology of thermoplastic polymers are of considerable importance from both a basic and a practical point of view. Spherulite size, size distribution, and microscopic morphological changes within the spherulites can be varied by thermal history or nucleating agents. Under special conditions, for example during the compression moulding of thick-walled parts, different local cooling conditions can lead to differences in the morphology across the whole thickness. In the regions of slowest undercooling (i.e. often the thickest portion of the parts), the morphology is coarsely spherulitic and contains individual voids and even holes. In the case of rapidly cooled and therefore mainly spherulite-free materials the flow-disturbance of the melt can lead to the occurence of the well-known flow lines. They are additional sites for crack nucleation aided by internal stresses as produced by contraction of the cooling polymer (Fig. 6).

To study the effects of various morphological features on the fracture behaviour of semicrystalline thermoplastics in more detail, a relatively low molecular weight, isotactic polypropylene (Novolen PP 1120 LX, BASF, Germany), containing 5% of randomly arranged blocks of atactic polypropylene, was used as the main testing material. With two other types of PP it was explored which changes in fracture behaviour can occur if (1) the molecular weight of the polymer is raised (PP 1120 HX) or (2) a material with a higher atactic content is used (PP 1320 L) [8].

Bulk sheets of these three types of polypropylene were subjected to different thermal treatments, which are more fully described elsewhere [9]. Briefly, quenching of the materials resulted in a fine-spherulitic structure, whereas isothermal crystallization at elevated temperature led to the formation of coarse spherulites. In most of the morphologies no differences between the individual types of polypropylene could be observed by optical microscopy. Only in the case of the coarse spherulitic structures the polymers with low atactic content (PP 1120 LX and PP 1120 HX) exhibited local voids at some triple points of the spherulites, which in some extreme cases had grown to become large holes in the morphology. On the other hand the boundaries in the analogous morphology of PP 1320 L with the higher atactic content were free of any visible defects.

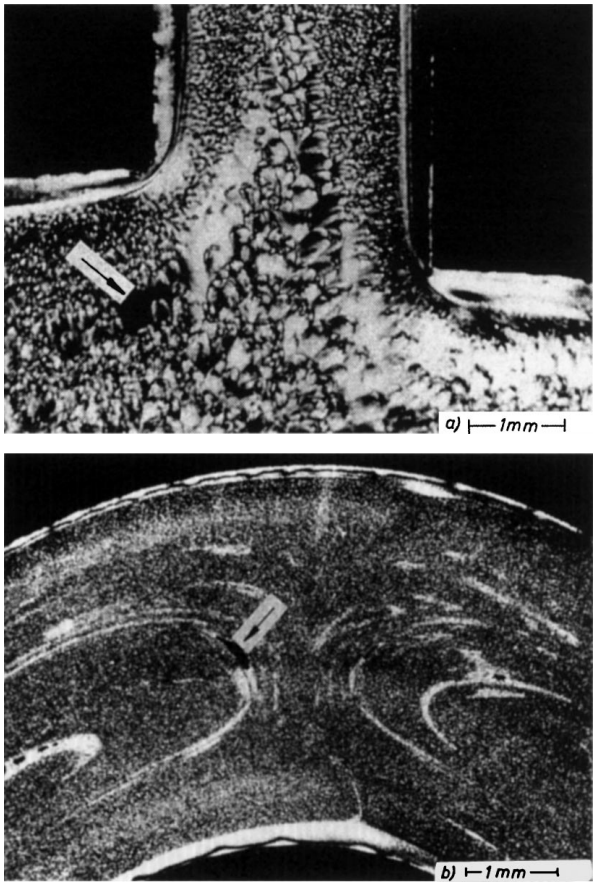

Figure 6 Faults in thermoplastic structural elements: (a) void in the coarse spherulitic interior of a T-joint (left) and (b) cracks along flow lines in the wall of a pipe (right).

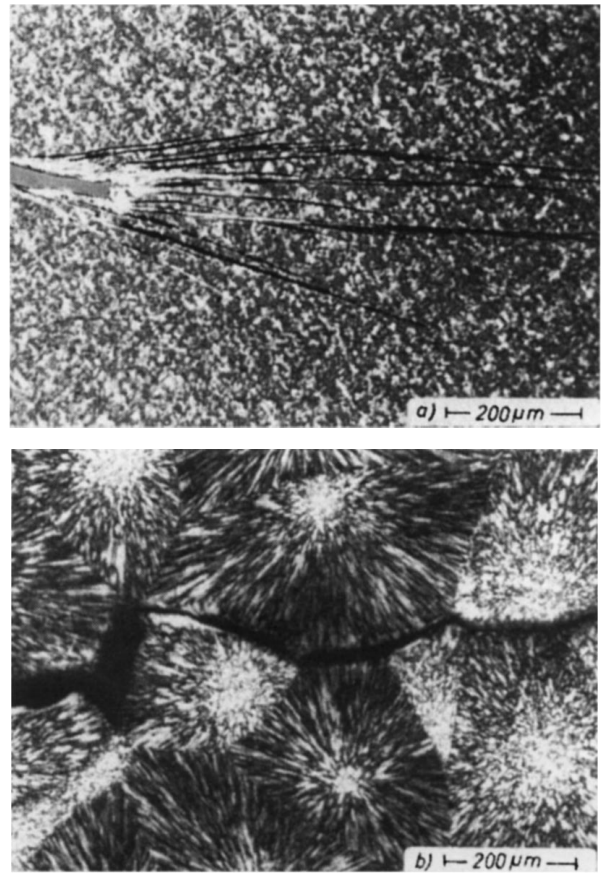

Figure 7 Polarized light micrographs of slow craze- and crack-initiation in PP 1120 LX with fine (a) and coarse spherulitic morphology (b).

TABLE I Mechanical properties of fine and course spherulitic polypropylene

Properties	Fine spherulitic (100 μm)	Coarse spherulitic (420 μm)	Literature reference
Strength (MPa)	34	15	30–33
Elongation at break (%)	150	7	100–200
Fracture toughness (MPa $m^{1/2}$)	4.6	3.5	3–4.5

PP 1120 LX (BASF).

As an example, Table I illustrates for the standard material 1120 LX the effect of spherulitic morphology on various mechanical properties. Drastic reductions in strength, elongation to break and fracture toughness are observed when the mesostructure contains coarse spherulites, interspersed with voids, with weak bonds across the spherulite boundaries. In addition, these reductions are associated with changes in the fracture mechanisms. In the fine spherulitic polypropylene crack propagation is chiefly controlled by the formation of crazes in front of the crack tip, while in the coarse spherulitic morphology cracks begin to propagate along spherulite boundaries before unstable, brittle fracture occurs (Fig. 7) [10]. These various mechanisms provide different morphologies of the fracture surfaces. They can exactly be attributed to the observed individual crack paths in the different microstructures. At the onset, the fracture surface of fine spherulitic PP 1120 LX has a smooth fibrillar structure which had formed during plastic deformation and final rupture in one of the sharp crazes. On the contrary, a polyhedron-shaped fracture surface was formed by the completely interspherulitic crack propagation in the slowly crystallized PP 1120 LX consisting of coarse spherulites with greater stiffness.

A final comparison of the individual types of PP with their different mesostructures (due to molecular, microstructural, and morphological parameters) can clearly be accomplished on a definition of "strength" as the product of yield or fracture stress and fracture toughness [11, 12]. If this product is compared with the yield stress usually used for the dimensioning of thermoplastic elements, the results lead to the optimum material property with respect to the resistance against plastic deformation and fracture (Fig. 8) [13, 14]. For the present case such an analysis would provide the following information:

1. In all the three types of polypropylene a good "strength" at a relatively high yield stress is achieved when a fine spherulitic morphology predominates. This condition guarantees a high security against fracture, even at lower temperatures.
2. The best values of "strength" are found in the material with higher molecular weight.
3. Both "strength" and yield stress decrease severely with increasing coarseness of the morphology.
4. The degradation of these properties is reduced if a polymer with higher atactic content is used.

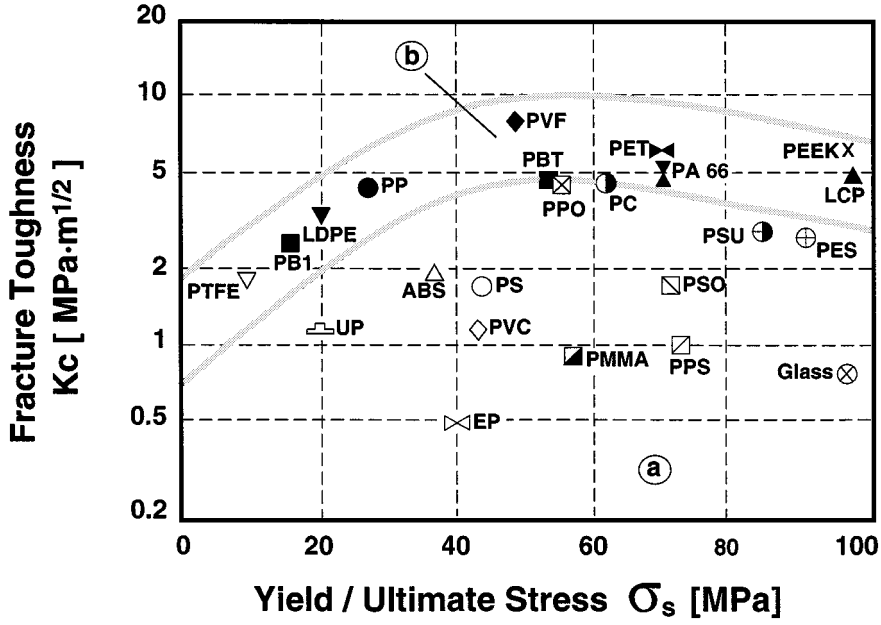

Figure 8 Comparison of fracture toughness and yield/ultimate stress of some amorphous (a) and partially crystalline polymers (b) [12–14].

5. At the same time this molecular parameter provides a minor lowering of "strength" and yield stress of the fine spherulitic morphology.

In summary, it can be stated that in semi-crystalline isotactic polypropylene the sensitivity to crack propagation can be lowered by the right choice of the molecular composition (atactic content, molecular weight) and by a controlled production of a certain morphology.

3. Fatigue crack propagation in CTBN/EP-blends

A significant improvement in toughness of neat epoxy resins (EP) can be achieved by modifying them with reactive group-terminated acrylonitrile-butadiene copolymers (liquid nitrile rubber (NBR)), especially by their epoxy- or amine-prereacted carboxyl-terminated (CTBN) derivatives [15]. The rubbery domains formed by phase separation of the liquid NBR in the EP-matrix increase the toughness, but sacrifice its stiffness and decrease its glass transition temperature (T_g). The absolute changes in these properties, especially in fracture toughness, depend, however, on the mean size and size distribution of the dispersed phase inclusions [16]. On the other hand, to set the desired particle size by the phase segregation process (as being induced by curing in liquid NBR modified expoxies) requires not only a proper selection of the components, but also a fundamental know-how reflected by mesostructures.

Investigations of the effects of morphology of such blends on their toughness performance were mostly carried out under static loading conditons. Much less attention was paid to the fatigue crack propagation (FCP) behavior of toughened EP resins, although the effects of modification should be clearer and more informative in this case. Therefore, the following results give an idea about how various phase geometries affect the FCP-behavior and related failure phenomena in an EP resin modified by liquid carboxyl-terminated NBR (CTBN) of different amounts [17].

TABLE II Composition and properties of various CTBN/EP blends

Composition	Modifier content (phr)[b]	T_g (°C)	E (GPa)
Epoxy Resin EP (Epon 828)[a]	0	145	2.95
EP + Carboxyl-	5	135	2.84
terminated	10	128	2.38
nitrile rubber	15	120	1.95
(Hycar CTBN)	20	117	1.85

[a]Anhydride-cured EP-resin at a curing proportion EP: curing agent of 1 : 0.9.
[b]phr = parts per hundred resin.

Table II lists the various compositions tested, along with their glass transition temperatures and their elastic moduli. Up to a modifier content of 15 phr the CTBN-phase had a spherical particle shape (Fig. 9a). However, the morphology of the EP with 20 phr CTBN was no longer a dispersion type one. Instead, the rubbery phase tended to build up a coarse interpenetrating network structure (Fig. 9b).

In Fig. 10 it is clearly visible how the modification of the EP-matrix with CTBN improves its resistance to fatigue crack growth. The range of the data points plotted can be described adequately by the Paris-Erdogan power law:

$$\frac{da}{dN} = A \cdot (\Delta K)^m \tag{1}$$

where A and m are constants describing the position and slope of a linear fit to these data in a $\log(da/dN)$ vs. $\log(\Delta K)$ diagram. The arrow at the upper end of each curve indicates the transition from fatigue crack growth to crack instability (ΔK_{max}). Modifying the EP with CTBN shifts the FCP curves toward higher ΔK values and considerably lowers at the same time the exponential term "m". Increasing the amount of CTBN

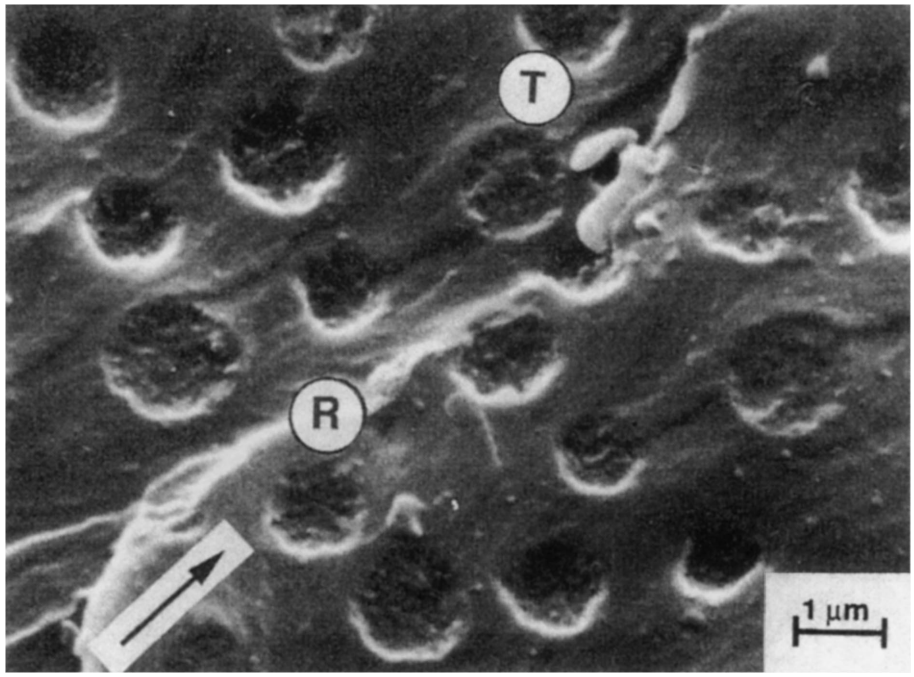

(a)

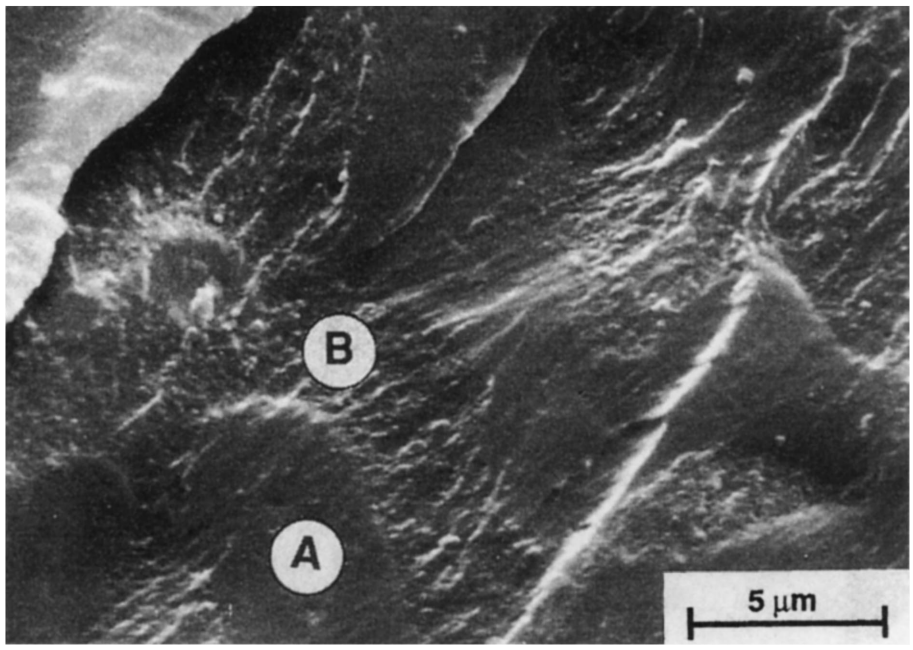

(b)

Figure 9 (a) Cavitated CTBN-particles on the fatigue fracture surface of CTBN-modified EP. Designations: arrow indicates crack direction, "T" tail formation and "R" microridges (due to crack propagation in slightly different planes), respectively. (b) SEM picture suggesting the existence of an interpenetrating network structure, taken on the fatigue fracture surface of the EP containing 20 phr CTBN (B).

improves the resistance to FCP in agreement with other results achieved on amine-cured EP resins [18].

The fatigue fracture surface of the 5 to 15 phr CTBN-modified EP showed stress-whitened regions composed of fracture steps and holes (or cavities) caused by the presence of the spherical modifier (Fig. 9a). In addition, it was perceptible that the cavities were filled by remnants of the rubbery modifier. Their topography shows that the improvement in FCP due to the presence of CTBN-particles was based on two effects:

(a) a process of pinning of the fatigue crack growth front when meeting locally the CTBN-obstacles, and

(b) an internal cavitation of the dispersed phase before being torn apart [17].

The build up of a network structure in the 20 phr CTBN/EP-system decelerated the fatigue crack growth even more efficiently than the particles did (even when the 5 phr higher amount of CTBN is not considered). Its high resistance to FCP can be attributed partly to a real crack-tip blunting process, in which rubber tearing and stretching of CTBN-network phase belong to the main energy dissipation processes. This is, however, not believed to be important in the case of rubber-modified EPs with fine particle dispersions, but seems to work in

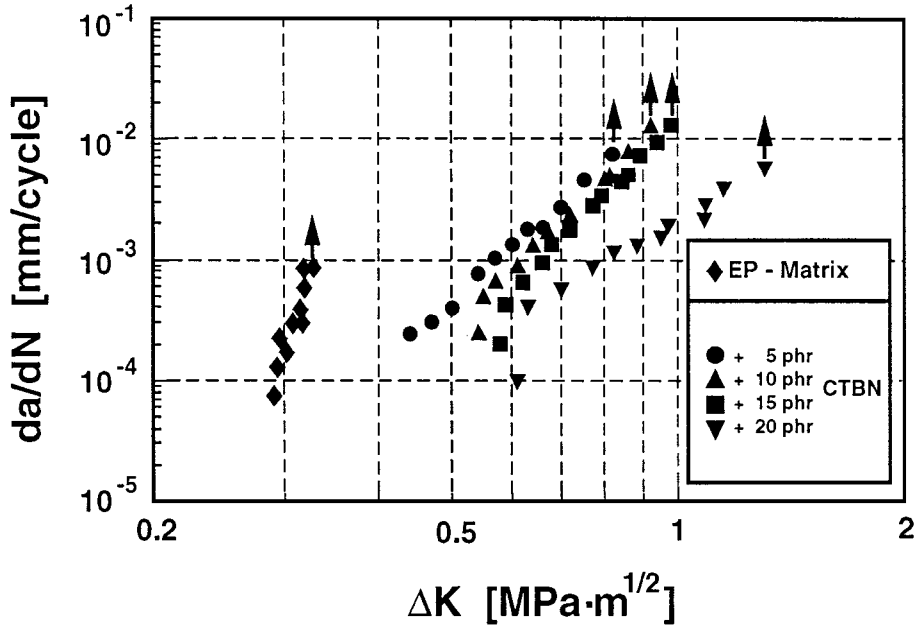

Figure 10 FCP curves of the neat and with CTBN-modified EP. Note: arrows indicate for ΔK_{max}, i.e. onset of crack instability.

dispersed systems with coarse rubber particles having diameters larger than 6 μm [19]. The interpenetrating network (IPN) structure may therefore be treated as an analogy to a dispersed one with coarse particles which allow bridging phenomena to occur.

In conclusion it can be stated here, that the observed phenomena can be considered as having taken place at the very low part of the mesostructure range (1–30 μm). Mesoscopic tailoring of the material for high fatigue crack growth resistance would mean to blend the EP matrix with an amount of CTBN rubber that allows us to maintain certain values of T_g and E, and at the same time to chemically modify the system in such a way that the rubbery phase builts up a coarse interpenetrating network structure.

4. Orientation order and fracture toughness of injection molded short glass fiber/PET matrix composites

Injection moulded short fibre reinforced thermoplastics are amongst the most complex of composite materials. In their final moulded form, they are typified by misaligned arrays of various length fibres dispersed in a viscoelastic matrix. The orientation of the short fibres is determined by the flow characteristics of the melt, which in turn depend on the mould geometry, the wall thickness of the final parts, the characteristics of a moulding operation, and the length and fraction of fibres in the composite [20]. One of various promissing developments of fibre reinforced thermoplastics (FRTP) is a commercial short glass fibre/thermoplastic polyethylene terephthalate (PET) system (Rynite®, DuPont, USA). With its composition including 45 weight per cent (wt %) glass reinforcement it belongs to the group of fibre reinforced thermoplastics with highest stiffness, and it can be processed in standard injection moulding machines without any problems. These and various other advantages of Rynite have led to advanced technical applications of this composite in, for example, the automotive industry.

For the design of parts for such applications it is of high importance to know more about the relationships between mesostructural details of these materials, their mechanical properties, and their failure behavior. The following results elucidate these facts on the example of a 45 wt % GF/PET system. Changes in the mesoscopic structure as a function of plaque thickness and their influence on fracture toughness under static loading conditions are illustrated. Wetherhold *et al.* [21] have shown that in this kind of short fibre reinforced thermoplastic matrix system the fibre orientation does change, more or less, through the thickness direction from place to place. However, roughly seen, three main layers of similar orientation exist. The presence of the mould surfaces had caused alignment of the fibres in the mould fill direction (MFD), while the centre section away from the surfaces contained fibres which were distributed more transverse to MFD (Fig. 11). An evaluation of the approximate dimensions for thicknesses of the aligned fibre boundary layers and centre layers indicates that, in general, the boundary layers seem to reach a fixed thickness for any plaque more than about 0.25 in ($\approx$6.35 mm) thick. Above this limit the centre layer contributes more to the cross-section of the plaques than the sum of both surface layers. This fact has an important influence on the mechanical properties of the material.

The effect of thickness B on the fracture toughness K_c is shown in Fig. 12. With increasing value of B the observed difference in K_c between cracks transverse (T) and longitudinal (L) to MFD, as measured for 1/16 in. (1.59 mm) thick plaques, decreased continuously until a point is reached where L-cracked specimens have a much higher K_c value than those with cracks in the T-direction. The transition seems to be due to the observed variation of the C/B ratio with plaque thickness. Specimens for which the centre layer C,

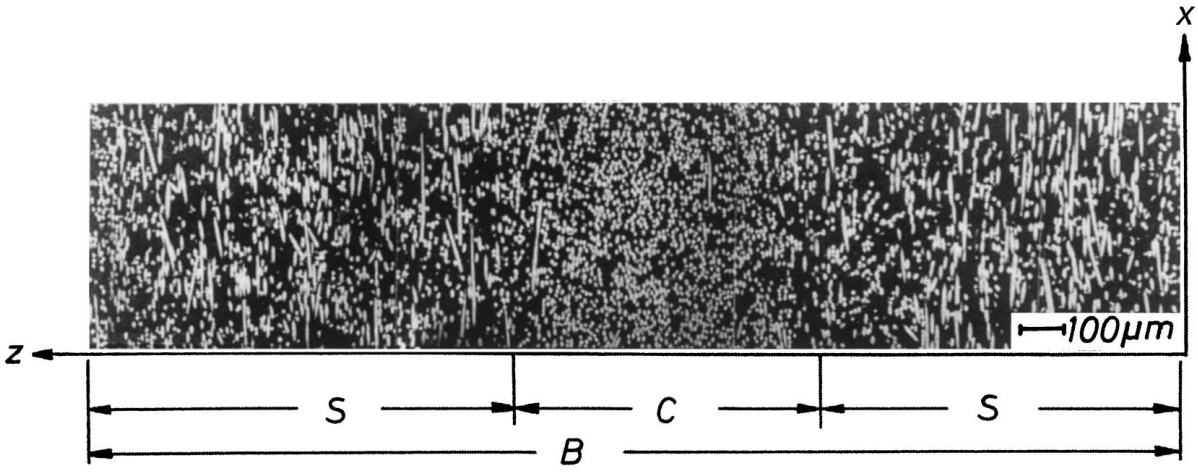

Figure 11 SEM micrograph of the layer structure in the *x*-*z* plane of a 45 w/o GF-PET composite.

oriented transverse to the surface, becomes larger than $B/2$ show exactly the opposite crack characteristic to that which would be expected from the orientation to the fibres at the surfaces. The change in crack characteristic for both crack directions is additionally superimposed on the well-known thickness dependence of K_c. This is due to a change in stress field condition with B (plane stress changing towards plane strain condition) accompanied by a tendency from macroscopic shear to a normal fracture mode [20].

The results of Fig. 12 have shown that the tendency and degree of the variation in toughness are mainly a function of the initial fracture toughness of the base polymer and several microstructural effects related to the fibers and the fiber/matrix interface. In a very simple approach, the composite's fracture toughness can therefore be described by a relationship of the form

$$K_{cc} = M \cdot K_{cm} \tag{2}$$

where K_{cm} is the fracture toughness of the matrix (PET here: $K_c = 2.5$ MPa $m^{1/2}$) and M is a "mesostructural efficiency factor". The latter depends upon fiber volume fraction, fiber orientation distribution ($\cong$ orientation order) over the cross-section fractured. In addition, M must be affected by the deformational behavior of the matrix material and the relative effectiveness of all the energy-absorbing mechanisms during breakdown of the composite.

In order to discuss these fundamentally different factors of influence on M, separately, a splitting of M in the form

$$M = a + n \cdot R \tag{3}$$

is useful. In this equation, the "reinforcing effectiveness parameter" R is the term which is directly related to the volume fraction of short fibers (V_f) and their geometrical arrangement across the plaque thickness ($R \geq 0$).

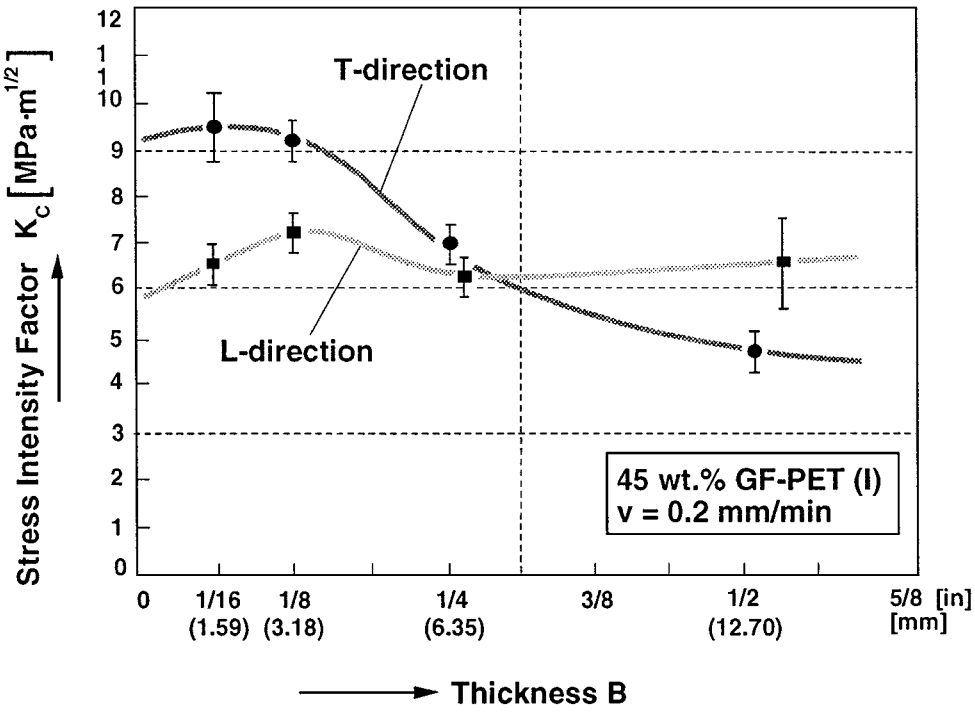

Figure 12 Variation of fracture toughness, K_c, with specimen thickness, B, of GF-PET composites.

As this arrangement is different for cracks in the L, as compared to those in the T-direction, R has to be calculated in the following ways:

$$\text{T-cracks: } R = \left(\frac{C}{B} \cdot f_{\text{p}\parallel\text{eff}} + \frac{2S}{B} \cdot f_{\text{p}\perp\text{eff}}\right) \cdot V_{\text{f}} \quad (4)$$

$$\text{L-cracks: } R = \left(\frac{C}{B} \cdot f_{\text{p}\perp\text{eff}} + \frac{2S}{B} \cdot f_{\text{p}\parallel\text{eff}}\right) \cdot V_{\text{f}} \quad (5)$$

In these correlations, the effective fiber orientation factors $f_{\text{p}\parallel\text{eff}}$ and $f_{\text{p}\perp\text{eff}}$ $(0 \leq f_{\text{peff}} \leq 1)$ express the hindrance effect of fibers due to their local orientation in the different layers C/B and $2S/B$ with respect to the actual crack direction. Further details, also about the "matrix stress condition factor" a (with $a \approx 1$) and the "energy absorption ratio" n, can be found in [22].

A plot of the normalized fracture toughness values of the composites against the reinforcing effectiveness parameter R along with additional results from other studies [22, 23] yields the following informations on how mesostructural parameters must be changed, in order to optimize the material's fracture toughness (Fig. 13):

(a) If the slope n is held constant, R as a function of fiber orientation and orientation order can be varied by:
- i) plaque thickness,
- ii) 'injection molding conditions (temperature, pressure, etc.),
- iii) flow field conditions as a function of gate and mold geometry,
- iv) fiber volume fraction,
- v) relative crack and load directions.

(b) At a constant R value, an enhancement of n is possible by manipulating one or more of the factors:
- i) fiber aspect ratio,
- ii) stress-strain behavior of the matrix without changing K_{cm},
- iii) interfacial bond strength,
- iv) fiber strength and stiffness.

In some way, of course, the individual factors are interrelated so that changes in one direction may also give changes in the other direction. Thus, a permanent control of the resulting changes in fracture toughness of the composite is always necessary for the final material development and the optimization of their properties through mesostructural design.

5. Packing effects on fatigue behavior of discontinuous aligned fiber composites

Polymers reinforced with aligned discontinuous carbon fibres are not only of interest from the viewpoint of recycling of scrap resulting from manufacturing of continuous fiber reinforced prepregs, but also because they can be considered as potential materials for structural components; they can be manufactured into complicated shapes with simultaneous satisfactory mechanical properties. A high alignment of the fibres yields an improvement in strength and stiffness of the composites in the fibre direction, so that the anisotropy of the properties of these materials is enhanced. This means that at the same time a reduction in the mechanical properties perpendicular to the fibre direction takes place. However, using the laminate technique which has been applied successfully in the design of materials with continuous fibres, prepregs of aligned discontinuous fibres can also be layered at different angles and be combined with each other in an autoclave or compression molding process. In this way material design can be

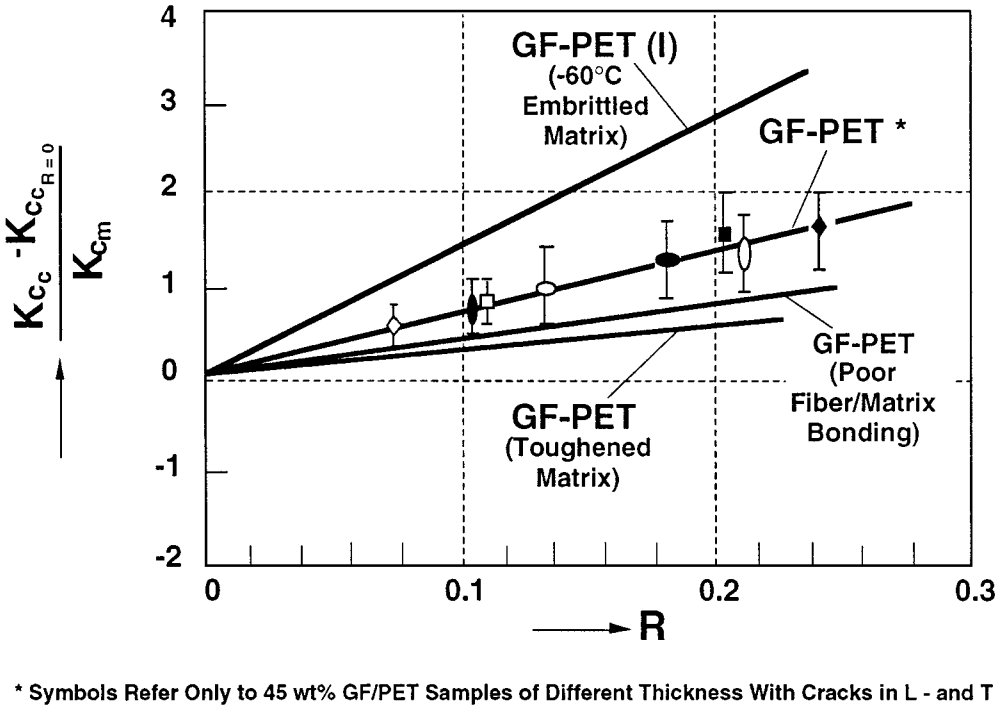

Figure 13 Relative changes in fracture toughness (ΔK^*_{cc}) of various thermoplastic matrix composites with increasing "reinforcing effectiveness factor" R.

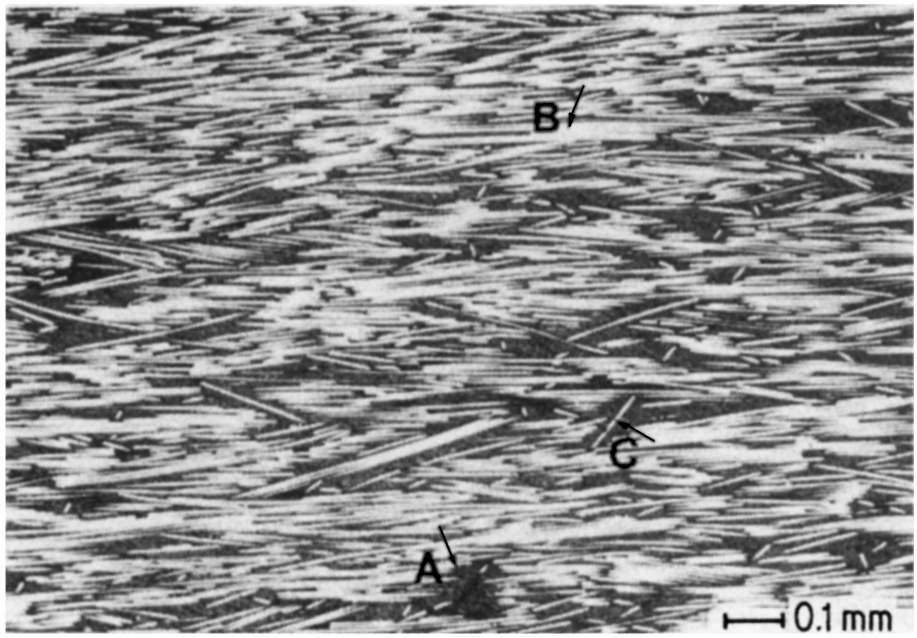

Figure 14 Polished cross-section of a PES $[0]_8$ laminate parallel to the fibre direction, showing resin-enriched regions (A), fibres of high degree of orientation aligned within separated fibre bundles (B), and individual misoriented fibres (C).

performed under the consideration of the loading conditions expected. Due to the nature of fiber discontinuity, however, the probability of variations in mesostructure is much higher than expected for continuous fiber composites. To study the effects of these mesostructural variations on the mechanical behavior in more detail, a discontinuous aligned carbon fiber/PES-system was subjected to tensile fatigue loading conditions [24]. Alignment of fibers, having a length of about 3 mm, was performed by the use of the vacuum drum filter technique developed in the central laboratory of former MBB (now Daimler Benz), Ottobrunn, Germany [25]. The degrees of alignment and orientation of the discontinuous carbon fibres are illustrated by the polished cross-section taken parallel to the fibre direction of a PES $[0]_8$ laminate in Fig. 14. Although fibre alignment has occured in the form of separated fibre bundles, it can be observed that locally individual fibres exhibit a high deviation from the main fibre direction. There also exist resin-rich regions at the ends of fibre bundles (with some evidence of end synchronization) as well as in the vicinity of misoriented individual fibres. During the preparation procedure of the laminates, void formation as a result of insufficient impregnation of the prepregs with matrix resin could not be avoided completely; in particular, the PES laminates possessed a relatively high void density.

Table III lists the measured tensile properties of unidirectional CF/PES-samples in comparison to theoretically calculated values using typical rule of mixtures approaches [26, 27]. Both the measured elastic modulus and the tensile strength are lower than the theoretical values, when loading occured in the fiber direction. The reductions are expected and due to the mesostructural details of the material. Regarding the modulus of the $[90]_8$-samples, on the other hand, a positive effect of the mesostructure is observed. Misorientation of the bundles and of individual fibers are mainly responsible for this difference relative to the theoretically calculated value. This is, however, not the case for the strength in the transverse direction; here, one difficulty is to exactly calculate the strength value from theoretical considerations, the other is that in spite of misoriented fibers the high void content in the composite and stress concentration sites at end-syncronized and non-end syncronized fiber bundles give rise to catastrophic failure at stresses lower than the strength of the neat matrix.

TABLE III Comparison between experimental and theoretical modulus and strength data of discontinuous aligned CF/PES composites

	Properties			
	E-modulus (GPa)		Strength (MPa)	
Material	Measured	Calculated	Measured	Calculated
PES-matrix	3	—	68	—
CF[a]/PES $[0]_8$	90	110	1000	1363
CF/PES $[90]_8$	7.2	5.9	46	62[b]

[a]Courtaulds XAS: $E = 242$ GPa; $\sigma_B = 2.75$ GPa; fiber length 3 mm, volume fraction 50%.
[b]Assumption of good F/M bonding and 4% voids.

Fig. 15 summarizes the results of fatigue tests with the PES-laminates [24]. The highest stress level to achieve failure after, for example, 10^6 load cycles is necessary for the $[0]_8$ laminate (a factor of about two higher than the failure stresses for the $[0, \pm 45, 0]_s$ and $[0, 90, 0, 90]_s$ laminates, and more than 20-fold higher than the values of the neat resin and the $[90]_8$ laminate). The slope of the ultimate failure curves for the different composites differs in the following way:

(a) For the $[0]_8$ laminate, the upper stress level necessary for failure in the range between 10^3 to 10^6 load cycles decreases linearly and only slightly, i.e. in a very narrow range between 720 and 650 MPa.

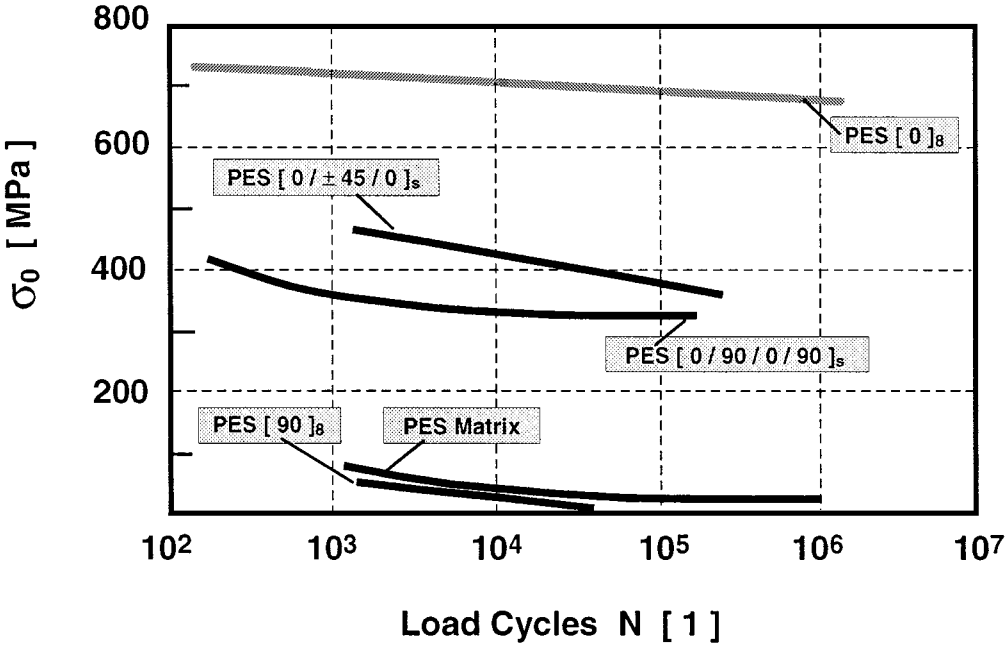

Figure 15 Variation of upper stress level for failure with number of cycles to failure, for various PES laminates and for the neat resin material.

(b) A continuous and steeper reduction of the upper stress level is observed for the $[0, \pm 45, 0]_s$ laminate down to a value of 350 MPa if an endurance limit of 5×10^5 load cycles is considered.

(c) At a slight lower load level as compared to the $[0, \pm 45, 0]_s$ laminates, the $[0, 90, 0, 90]_s$ laminates show a clear reduction of the upper stress limit in the range of low cycle fatigue (up to 10^4 cycles). In the region above $N = 10^4$ cycles, however, these curves tend to decrease only very slightly, as for the $[0]_8$ laminates.

(d) The neat PES resin as well as the $[90]_8$ laminate show a permanent reduction of the upper failure limit at the same, very low stress level.

A measure of the damage development in a laminate during fatigue loading is the change in stiffness during the load history. The variation in stiffness is determined by measurements of the secant elastic modulus. Schematically, the damage development in a $[0, 90, 0, 90]_s$-specimen and the simultaneous reduction in the secant modulus is illustrated in Fig. 16. Failure behavior of this kind of composite laminates starts at relatively low loads by the formation of individual transverse cracks (region 1). The number of cracks increases with increasing load until an equilibrium, characteristic damage state (CDS) is reached (region 2).

In region 3 a failure mechanism becomes effective which is typical for the existing mesostructure in discontinuous aligned fibre reinforced laminates. Starting from the specimen edges, longitudinal cracks are formed which propagate at an angle of about 2° to the load direction in the 0° layers until the specimen ends

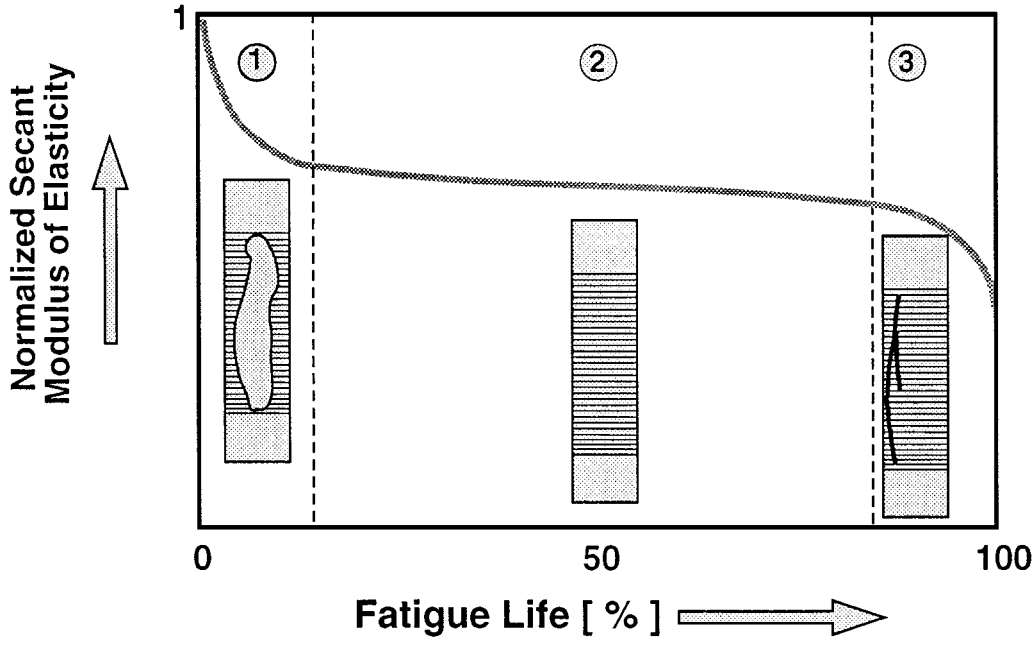

Figure 16 Schematic representation of damage development and simultaneous reduction in secant modulus of and $[0, 90, 0, 90]_s$ laminates during fatigue.

are reached. It is obvious that one reason for this angle is based on the alignment of the short fibres in bundles of about 75 μm in diameter and a length similar to the fibre length of 3 mm. It can be assumed that the cracks must usually follow these bundles (which in turn are not perfectly oriented) until they reach the bundle ends (end synchronization). Here, they can take the more favourable direction perpendicular to the applied load, i.e. through the resin-enriched regions. But this process is stopped soon by the interface of the next bundle, along which the crack is now forced to propagate. In fact, such a propagation mode results in an angle of crack direction which is very close to 2°.

At the edges of these longitudinal cracks further cracks are initiated at a later stage. The wedgelike fracture tips which are generated by this kind of longitudinal zig-zag crack progress finally delaminate the 90° layers adhering next to them, so that they are no longer capable of bearing any loads. Especially for this case a reduction of the load-carrying cross-sections of the external 0° layer by 10% results in an increase of load by about 2.6% in the residual 0° layers. This finally leads in a relatively short time to a complete failure of the specimen investigated. The initiation of these longitudinal cracks at the specimen edges and the crack edges, respectively, is especially favoured by (a) resin enriched regions; (b) poorly aligned fibres; (c) voids; and (d) ends of fibre bundles (Fig. 17). Therefore, to improve the fatigue performance of these systems a better control of the prepreg production process (including quality of impregnation and fiber alignment) is required in order to reach a more beneficial mesostructure.

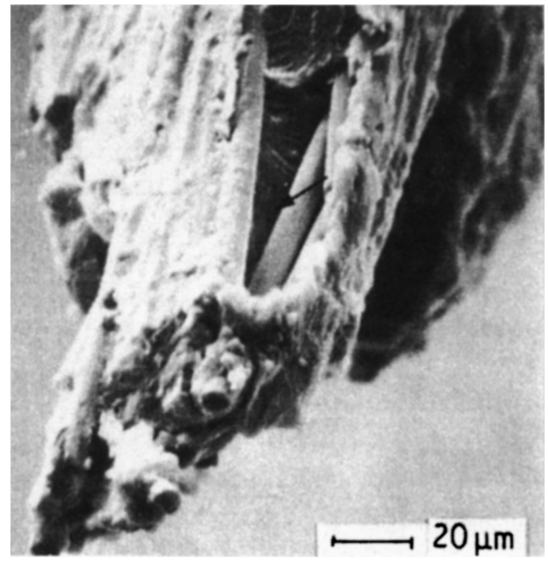

(a)

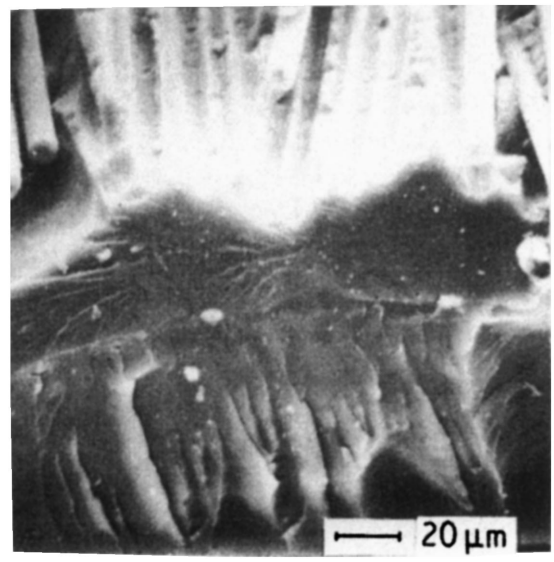

(b)

Figure 17 Scanning electron micrograph characterizing a typical site of longitudinal crack initiation in the 0° layers of PES fatigue specimens: (a) pores (arrow) due to poor impregnation at the end of a fiber bundle, building up a wedge-like fractured piece formed by the initiation of a new longitudinal crack on the edge of another one, which before ran in the opposite direction and (b) resin rich region.

6. Mesostructure and properties of pultruded continuous glass fiber/polypropylene composites

Commingled yarns are one of the possible preforms used for continuous fiber reinforced thermoplastic composites in order to solve the problem of high melt viscosity during impregnation and consolidation as the required steps for manufacturing of technical components. The preforms can be considered as "dry" prepregs, in which the solid thermoplastic polymer in form of fibers is physically divided and more or less evenly distributed among the reinforcement fibers (Fig. 18) [28].

The development of this kind of pre-impregnation technology for thermoplastic matrices has also generated considerable interest in the possibility of thermoplastic pultrusion [29–31]. Successful trials have however only been performed for simple cross-sections, and at pultrusion speeds not dramatically exceeding those known for commercial thermoset pultrusion (0.6–1.2 m/min). Major reasons for these deficits are the inherent difficulties associated with the thermoplastic matrices, such as high processing temperatures and high melt viscosities. An additional obstacle may be a lack of both fundamental understanding of the governing process mechanisms and adequate mathematical models for predicting the relationships between the various processing variables and the resulting structural/mechanical properties of the thermoplastic pultruded products [32].

The following studies were performed to elucidate the relationships between pultrusion parameters and the quality of parts made of commingled glass fiber/polypropylene fiber preforms [33]. A schematic of a typical pultrusion line is shown in Fig. 19 [34]. Fiber bundles are preheated in a hot air preheating zone and enter directly into the heated die. The cavity of the latter is tapered, and its angle can be varied without changing the final thickness of the beam. A water cooled die just behind the heated die is installed for further compaction and improvement of the pultrudate's surface quality.

Due to a variation of processing conditions (preheating temperature T_{ph}, heated die temperature T_{hd} and pulling speed v_p) the void content and the resulting mechanical properties of the pultruded beams reflected

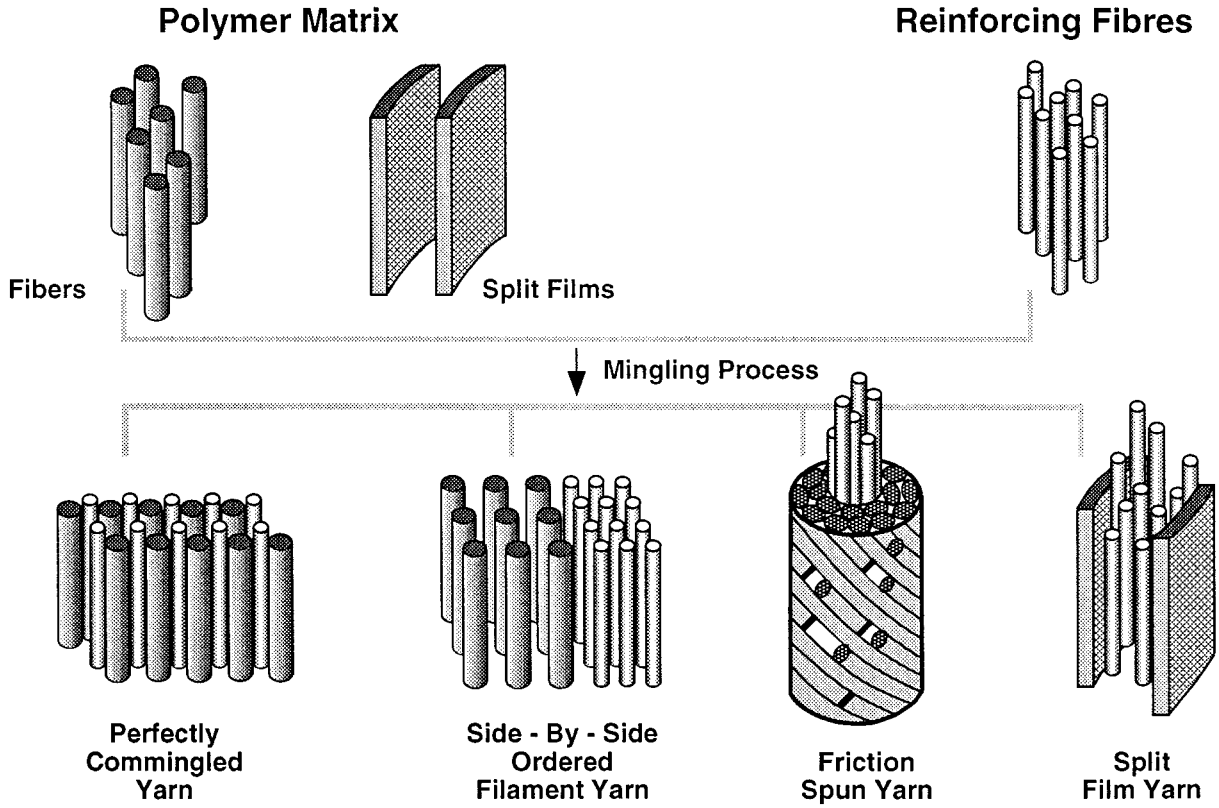

Figure 18 Schematic illustration of different hybrid yarn structures.

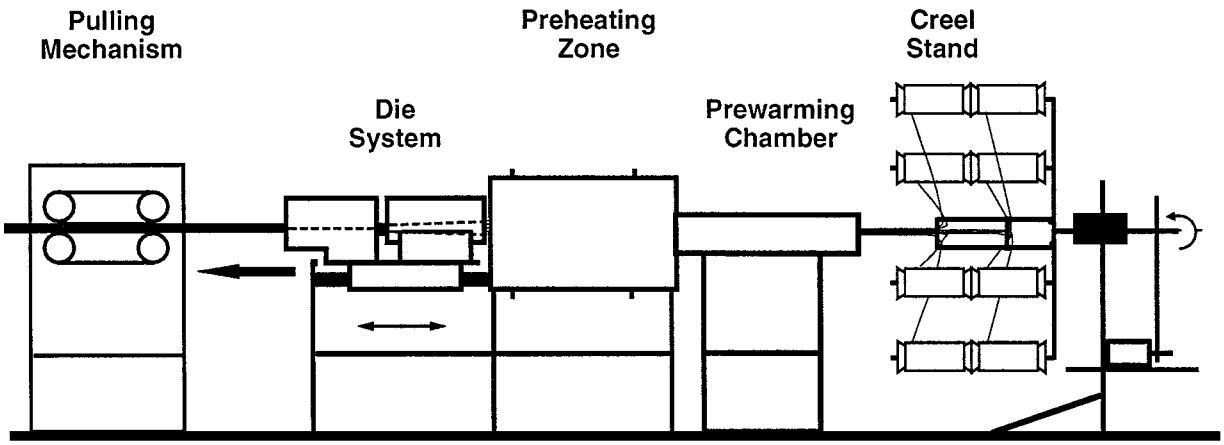

Figure 19 Schematic of the pultrusion line, used for the production of profiles.

significant changes. Fig. 20 shows qualitatively the influence of processing speed and processing time (i.e. time in the heated die) on the shear strength and the void content.

The latter, mesostructural feature was determined by the use of polished cross sections of the pultruded beams, that were evaluated by the use of an image analyser system. Fig. 21 illustrates the original micrograph of the GF/PP-cross section (a) and the void structure abstracted to a set of black spots by binarization of the grey values (b). It is now much easier to extract mesostructural information. Another mesostructural feature that results from the original mingling quality of the yarn material is the agglomeration of the reinforcing fibers between the matrix (Fig. 22). A finer dispersion of the reinforcing fibers not only leads to faster processing conditions, necessary for performing the impregnation and consolidation steps, but also to better properties of the final pultrudates. This mesostructual detail must also be considered when modelling the process with regard to predictions under which conditions of pressure, temperature, and time certain limits in void contents can be achieved [33–35].

7. Orientation disorder during stamp forming of curved components from continuous fiber/thermoplastic matrix composites

The existence of a melting/softening point in case of thermoplastic composites opens the possibility of producing intermediate forms, such as preconsolidated flat laminate panels, that can be processed or post-formed at a later data. One of the most attractive processing techniques in this respect is stamp forming [36]. The technique is rather similar to the sheet metal stamping process bearing the same name. In this process a

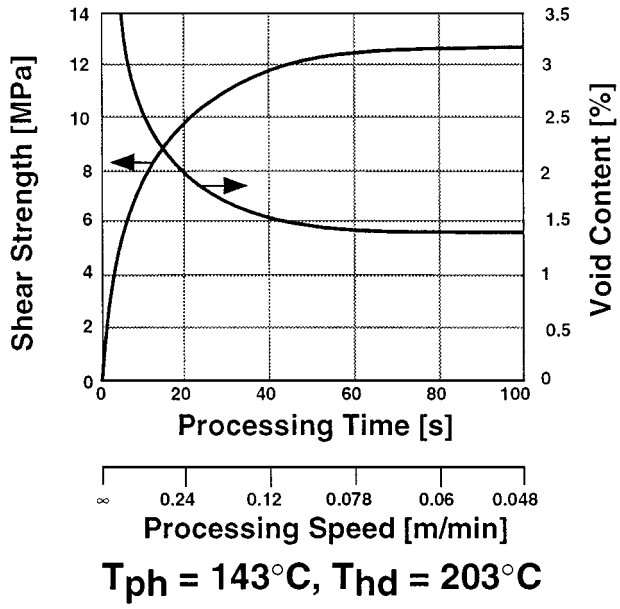

Figure 20 Shear strength at different processing times, $T_{ph} = 143\,^{\circ}C$, $T_{hd} = 203\,^{\circ}C$. Further improvements are possible (i.e. higher strength, lower void content) when increasing (up to a certain degree) the pressure, the preheating temperature and/or the temperature in the heated die.

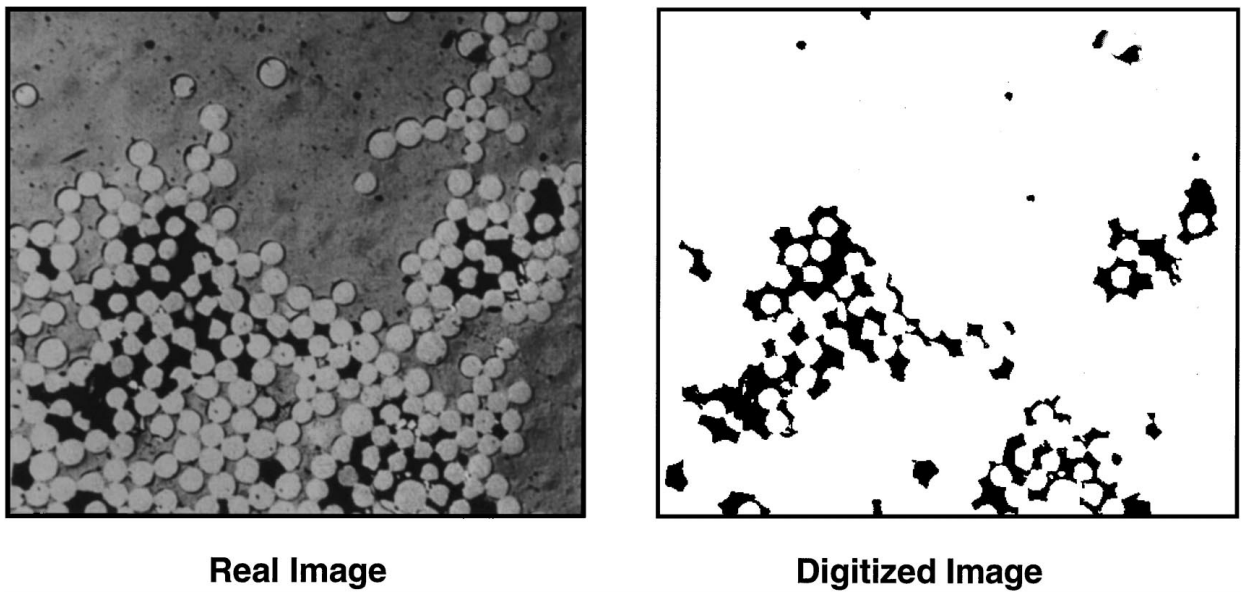

Figure 21 Scanning electron micrograph of voids between individual fibers of a poorly pultruded beam (left) and the digitized figure for image analysis (right).

semi-finished thermoplastic composite product, such as a preconsolidated flat laminate panel (which can be produced in a large series production procedure such as a double-belt press process [37]), is heated externally above the melting/softening temperature of the thermoplastic matrix; then the hot semi-finished product is quickly transferred into a cold mold where it is stamped to conform to the mold geometry.

The problem in all of these thermoplastic forming operations is that one has to stay within an optimum processing window (in terms of pressure, temperature, forming speed, and clamping conditions) in order to avoid defects in the material on a mesoscopic level. The defects, in turn, can result in deviations from the design criteria of the parts to be produced, including stiffness, strength, and geometrical constraints.

Based on previous works [38, 39], the following examples show how a continuous glass fiber reinforced polypropylene (GF/PP) system reacts when being stamp formed into two dimensional half tubes under various processing conditions.

Fig. 23 displays the geometry of the two dimensional mold. The male part (a) has a form of a "half" cylinder, while the female part (b) has a full half cylinder cavity. To prevent significant transverse flow of the composite material during forming into a half-tube shape, two sealings of silicon rubber were attached to both sides of the male part, thus forming a "closed" cavity with the female part. Both sides of the mold were additionally closed with flat metal plates (c). At a certain position between male and female part, there exists a uniform gap of 3.0 mm, which is equivalent to the thickness of the

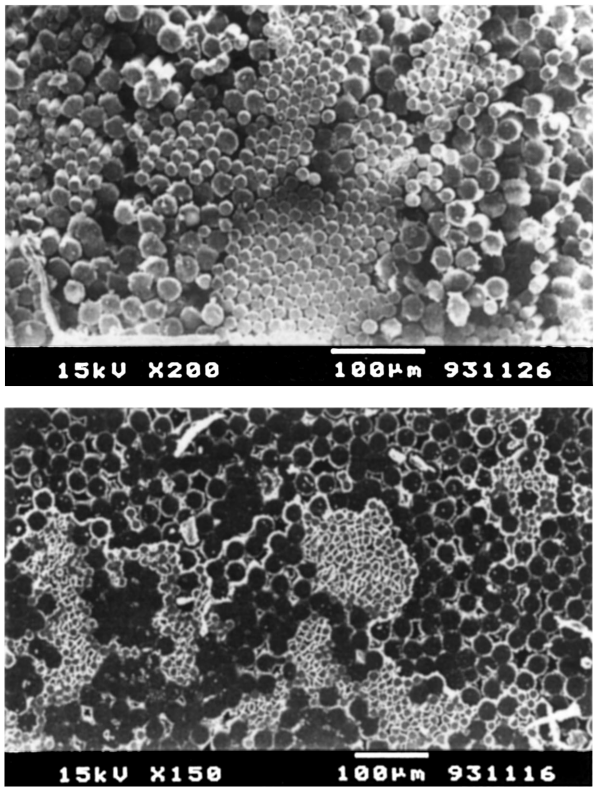

Figure 22 Fiber agglomerations of locally higher volume fraction than the one of the global pultruded specimen. The left SEM-photo shows an unconsolidated glass fiber/polypropylene fiber bundle (glass fibers have smaller diameter); the right SEM-photo shows a half consolidated glass fiber/polypropylene fiber bundle, having a finer mingling quality then in the left case.

originally flat, pre-consolidated GF/PP laminate panels. However, no stops were used to prevent the mold from closing beyond this point.

The typical forming procedure involves (a) heating the pre-consolidated laminate panel between two hot plates of an external hot press, to a temperature above the melting temperature of the PP matrix, without any external pressure; (b) quickly transferring the hot laminate panel into the forming system, which is kept at room temperature (transfer times are of the order of a few seconds to prevent significant cooling); (c) forming of the hot laminate panel into the final part, by utilizing the various speeds related to the closing and compression modes of the hydraulic press.

The composite forming cycle lasts for about 20 s; during this period the as formed part is cooled down by the cold mold under pressure. In the following removal from the forming system, the part has a temperature of about 30–40 °C. During the whole procedure the laminate panel remains embedded between two high temperature resistant, super-plastic films for better handling and forming conditions [40].

The stamping temperature as a function of closing speed and pre-heating temperature is plotted in Fig. 24. When the closing speed was higher than 70 mm/s, the achievable stamping temperature could be approximately maintained in one of the three ranges: I (180–185 °C), II (170–175 °C) and III (160–165 °C), depending on the pre-heating temperature of 190, 180 and 170 °C, respectively. Within each range, the value of stamping temperature was slightly higher the faster the closing velocity was. The corresponding fiber arrangements within the 2D samples formed in these three ranges are illustrated in Fig. 25a–c. Depending on the preheating temperature, out of plane fiber wrinkling and complete buckling of plies (a), inplane fiber waviness (or fiber "ripple" or "wash") (b), or favourable fiber alignment (c) were observed as typical mesostructural features of $[0]_6$ GF/PP samples formed within the temperature ranges of I, II or III respectively.

It is known from previous investigations that defects of type (a) and (b) also reduced the bending stiffness and strength of thermoformed v-shaped samples.

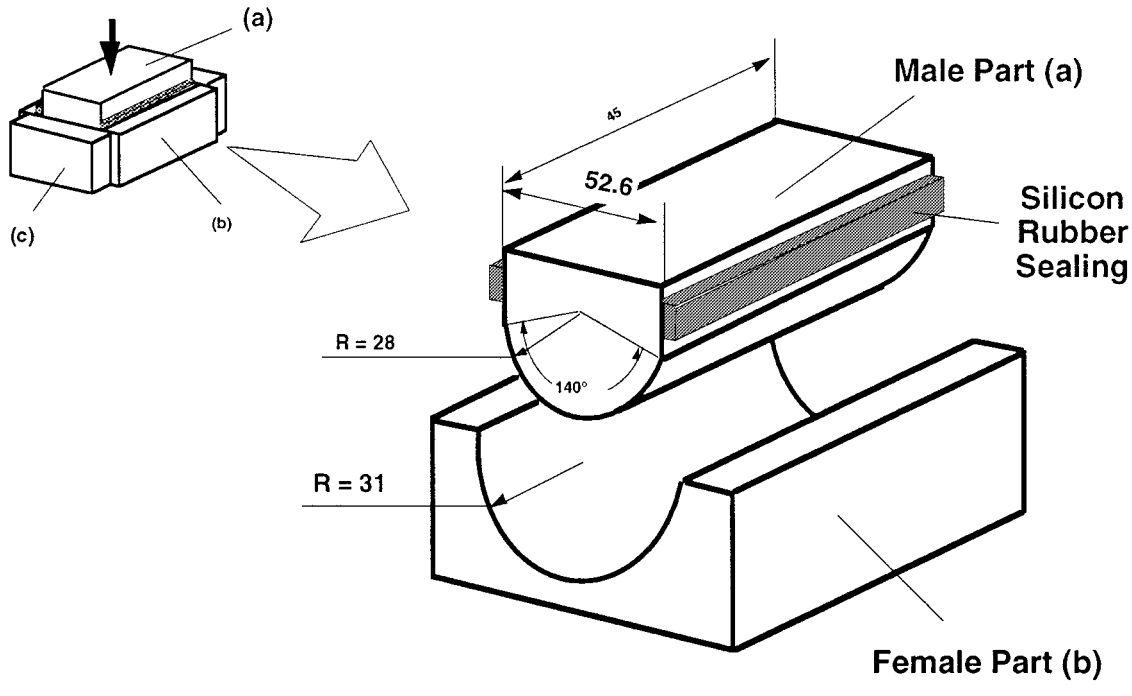

Figure 23 Mould geometry for 2D, half-tube samples.

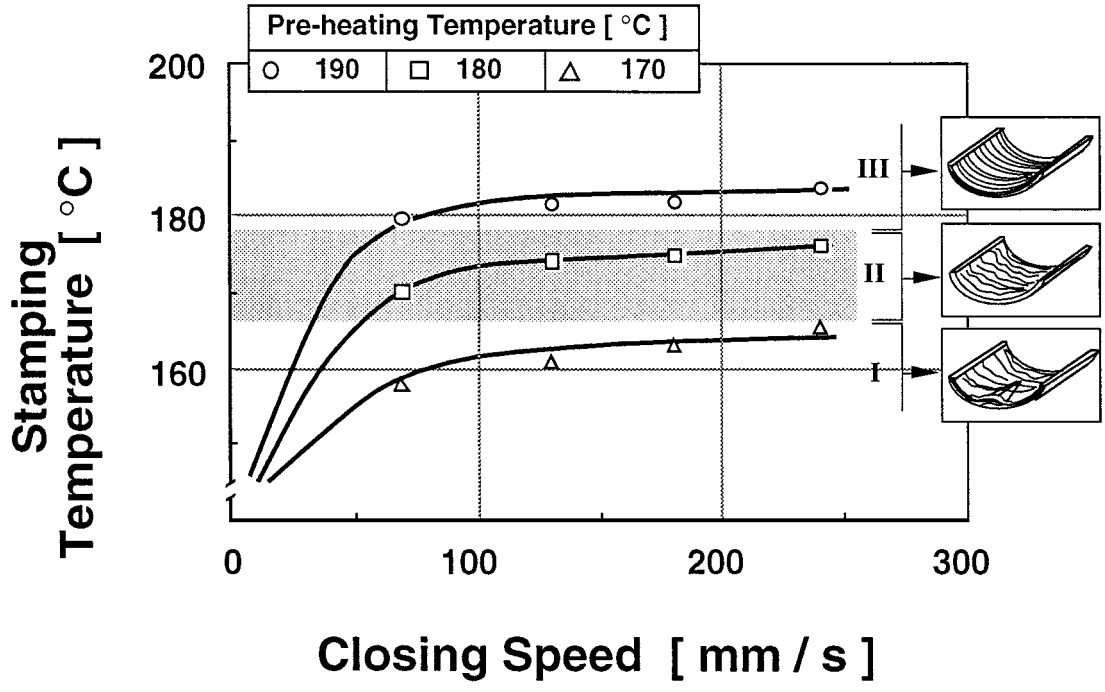

Figure 24 Stamping temperature as a function of closing speed and preheating temperature.

Other observations in this context refer to structural mesoscopic aspects, such as

(a) ply thinning in the bent region as a result of too high stamping pressures (especially if 90°-plies are existing in the laminate) [39],
(b) resin migration and resulting non-symmetric laminate structure (contributing to spring forward effects) [38],
(c) changes in fiber orientation of the individual plies (relative to the ones in the non-thermoformed plates) due to interply rotation effects during the stamp forming of crossply laminates into 3D-dome structures [38, 40, 41].

8. Concluding remarks on mesostructural design concepts and special mesostructures

It was shown by the previous 6 examples that matrix and fiber related details in the structure of discontinuous and continuous fiber reinforced polymer composites can highly affect their mechanical performance. As these structural details are found in a dimensional range between microstructure (on the lower micrometer scale) and macrostructure (characterized by the several millimeters to meter scale) they are called mesostructures. Most of the latter (about 90%) actually resulted from the conditions under which these materials were processed in order to build up a bulk component with a desired function and certain performance requirements. Therefore, to improve the properties, a strong control of the processing steps and conditions is needed so as to produce the most beneficial mesostructures. If, for example, toughness (besides a required stiffness) is the controlling property that has to be optimized for an injection moldable short fiber reinforced thermoplastic component with a given geometry and loading conditions, mesostructural design can be performed on various routes (Fig. 26) [42]. One is to modify the injection molding conditions in terms of gate position and geometry, mold temperature, back pressure, etc. The other is to modify the material by changing the fiber content, fiber length, toughness of the matrix, to mention only a few possibilities. Using, in addition, a software package for predicting the flow behavior of the melt and resulting orientation order of the fibers allows us to calculate via the mesostructural efficiency concept local fracture toughness at the most critical positions of the structural part. A comparison with the required toughness yields then information about if and how the mesostructure should be changed through the routes mentioned before. A similiar scheme can also be followed for the manufacturing of continuous fiber reinforced polymer composite components (Fig. 27), including decisions about the choice of the right manufacturing process, the type of pregregs or intermediate material forms, as well as temperature, time, and pressure conditions [43].

In addition, it should be mentioned here that some special mesostructures exist which are absolutely necessary in order to achieve for a material or component certain properties that are not possible without these mesostructures. These special mesostructures, in turn, can only be established if very specific processing techniques are applied. Four examples should be mentioned in this respect:

(a) Functionally gradient, particulate or short fiber filled composites, prepared either under centrifugal load [44, 45] or even under conventional shear loading conditions during injection molding (Fig. 28) [46].
(b) Polymer-polymer microlayer composites with high barrier properties, produced during blow molding of polyamide/high density polyethylene blends [47, 48].

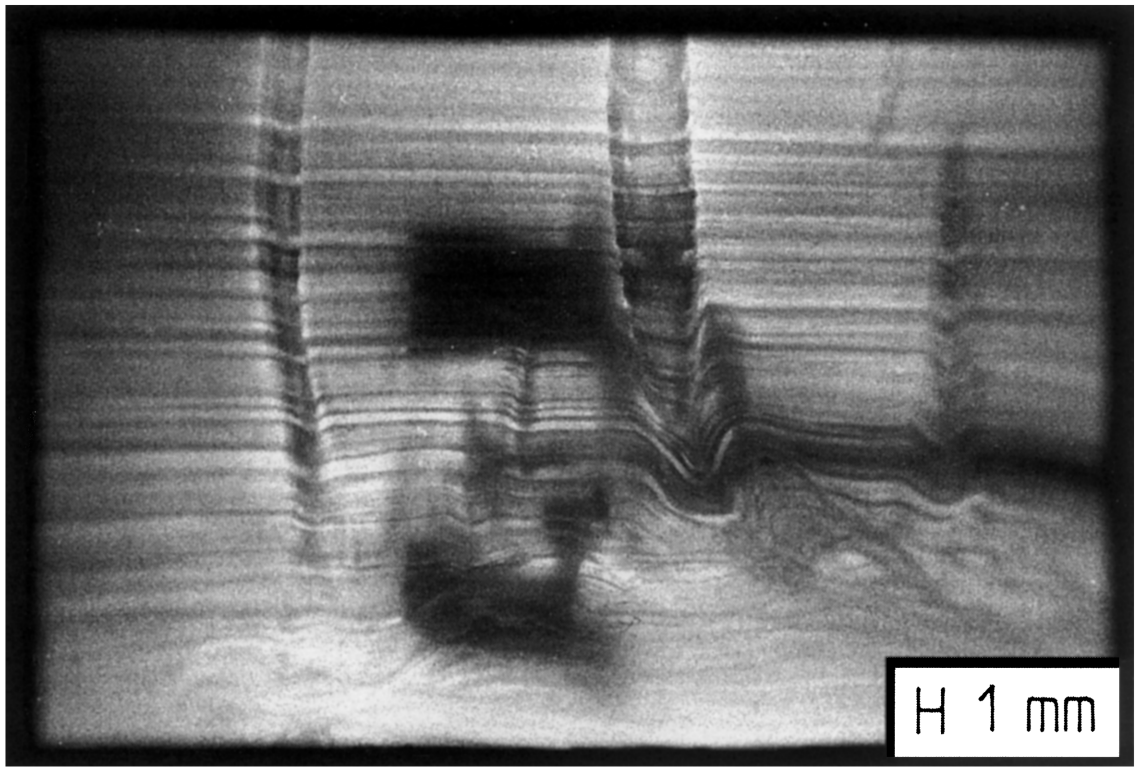

(a)

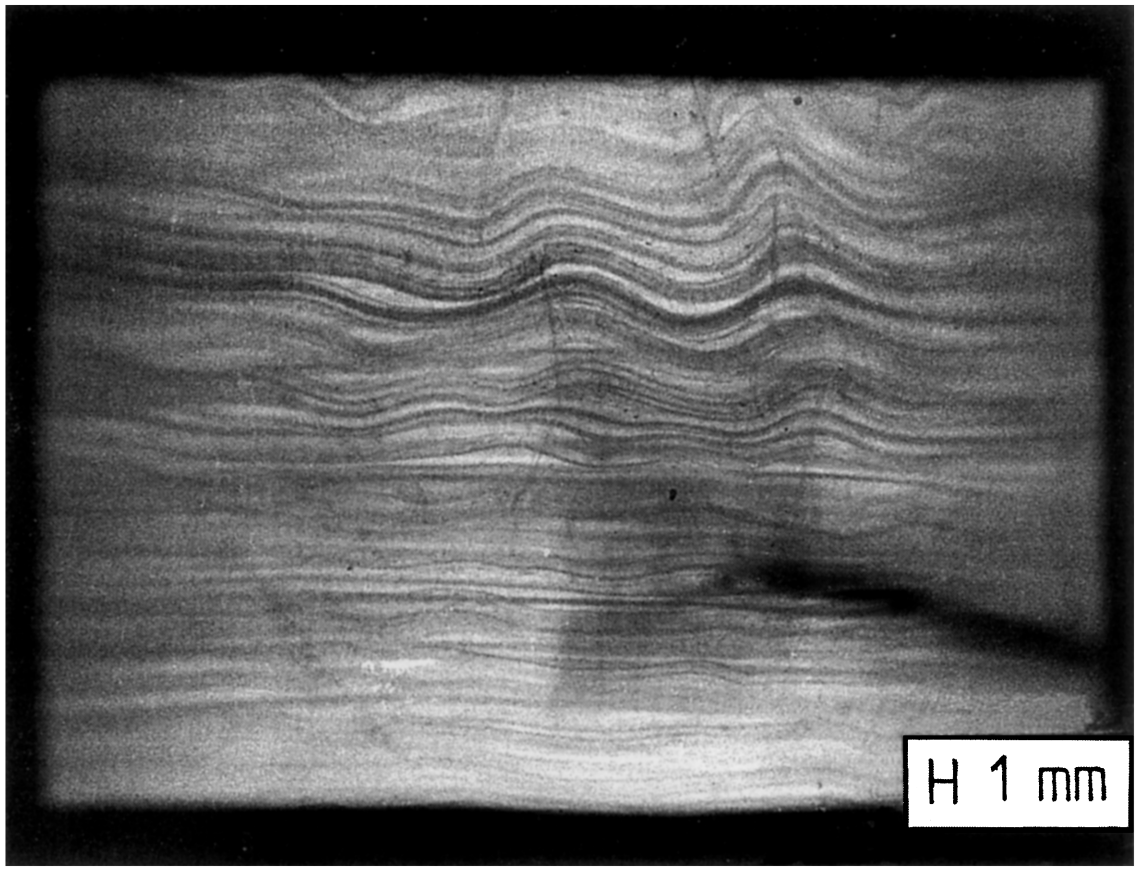

(b)

Figure 25 Microstructures of 2D samples, produced under various conditions: (a) Condition I, resulting in out of plane fibre buckling and in-plane fibre wrinkling. (b) Condition II, showing in-plane fibre wrinkling or fibre "ripple". (c) Condition III, leading to favourable alignment of fibres and desired interply slip phenomena. (*Continued*).

(c) "Living" or plastic hinges, as produced during injection molding of bulk polypropylene parts that are interconnected through a very thin channel (cross-section of the hinge). The two highly oriented layers with an almost isotropic layer in between (as a result of high melt velocity in this cross-section) are very fatigue resistant due to their quasi-hard elastic morphology [49].

(d) The manufacturing of microfibrillar composites (MFC) from blends of polycondensates' by extrusion, drawing, and isotropization [50].

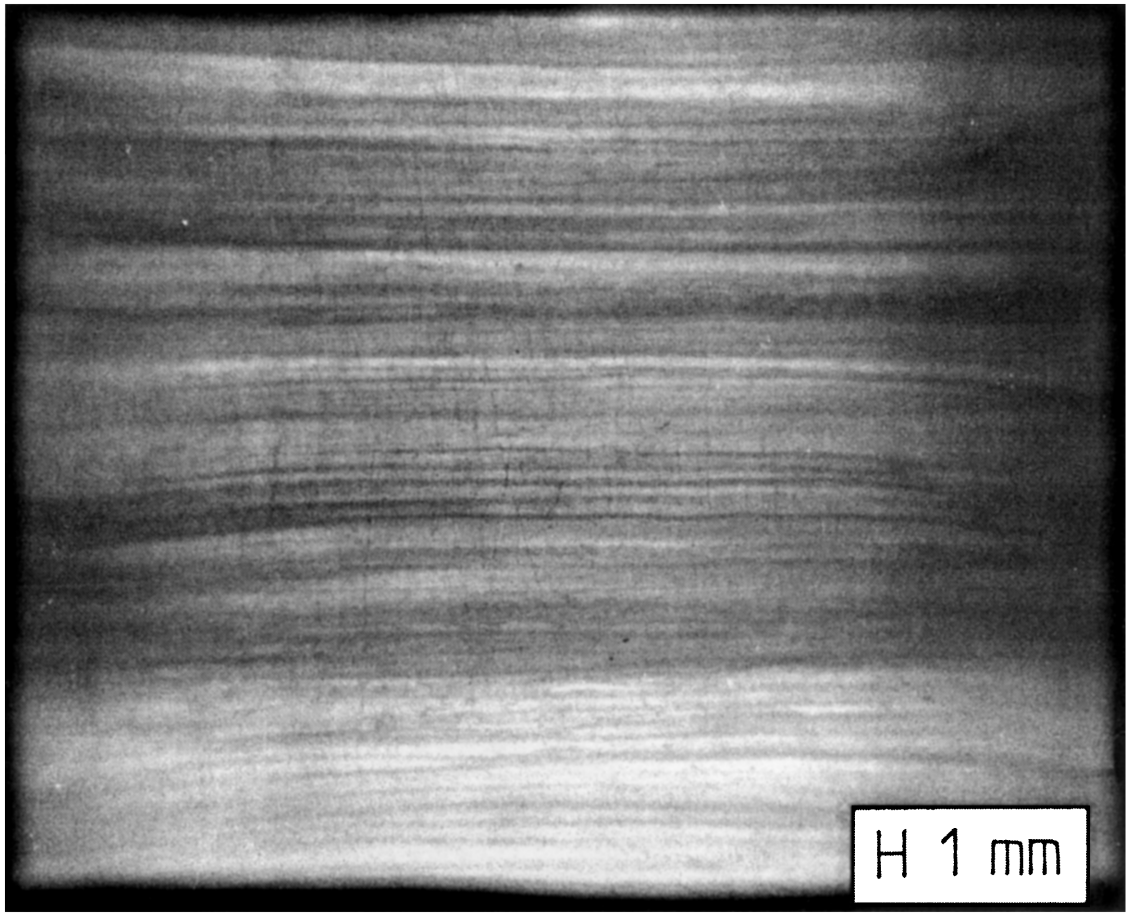

(c)

Figure 25 (*Continued*).

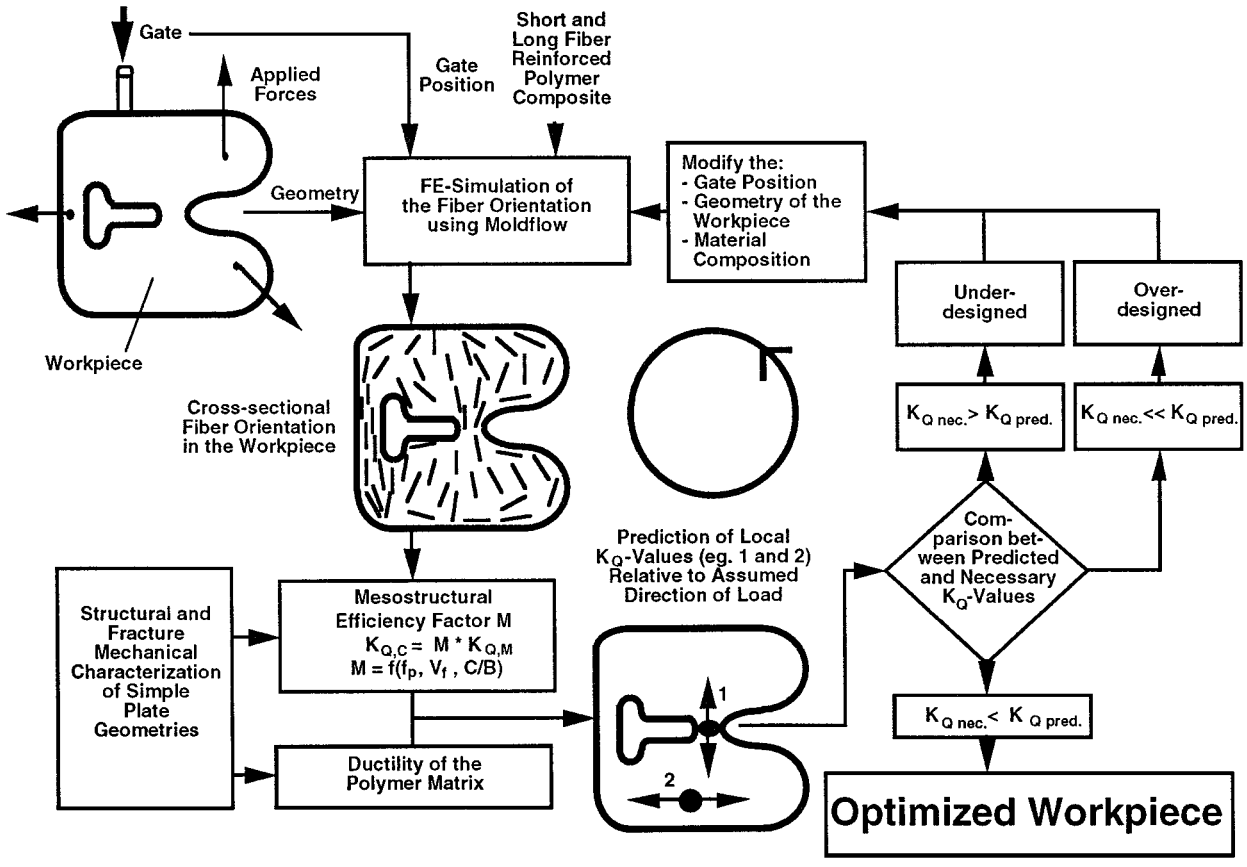

Figure 26 Scheme for prediction and optimization of local fracture resistance.

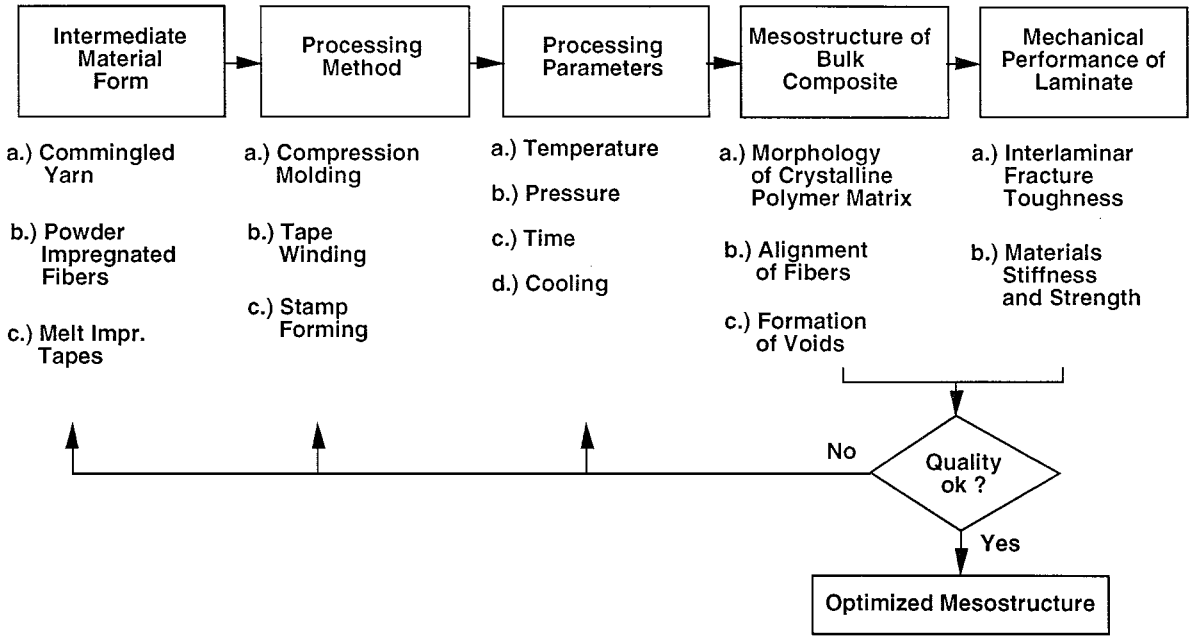

Figure 27 Methodology for fundamental studies on processing related properties of continuous fiber/thermoplastic matrix composite.

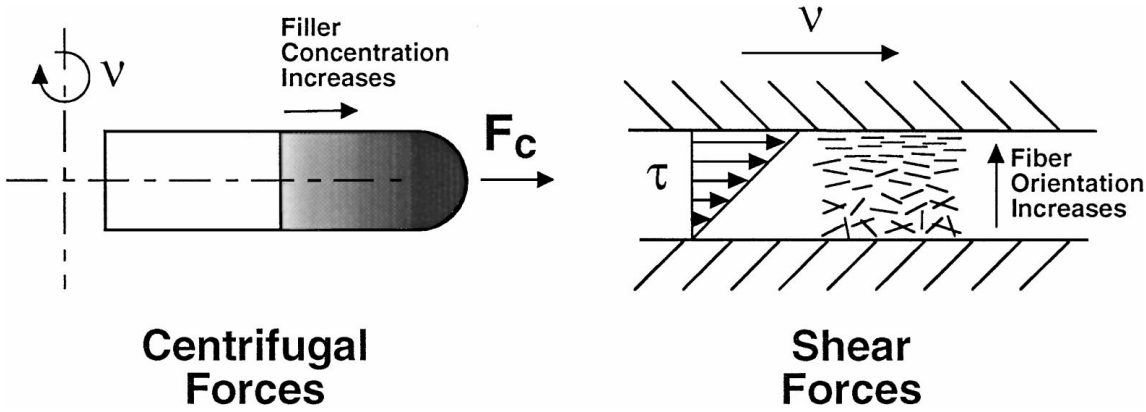

(a)

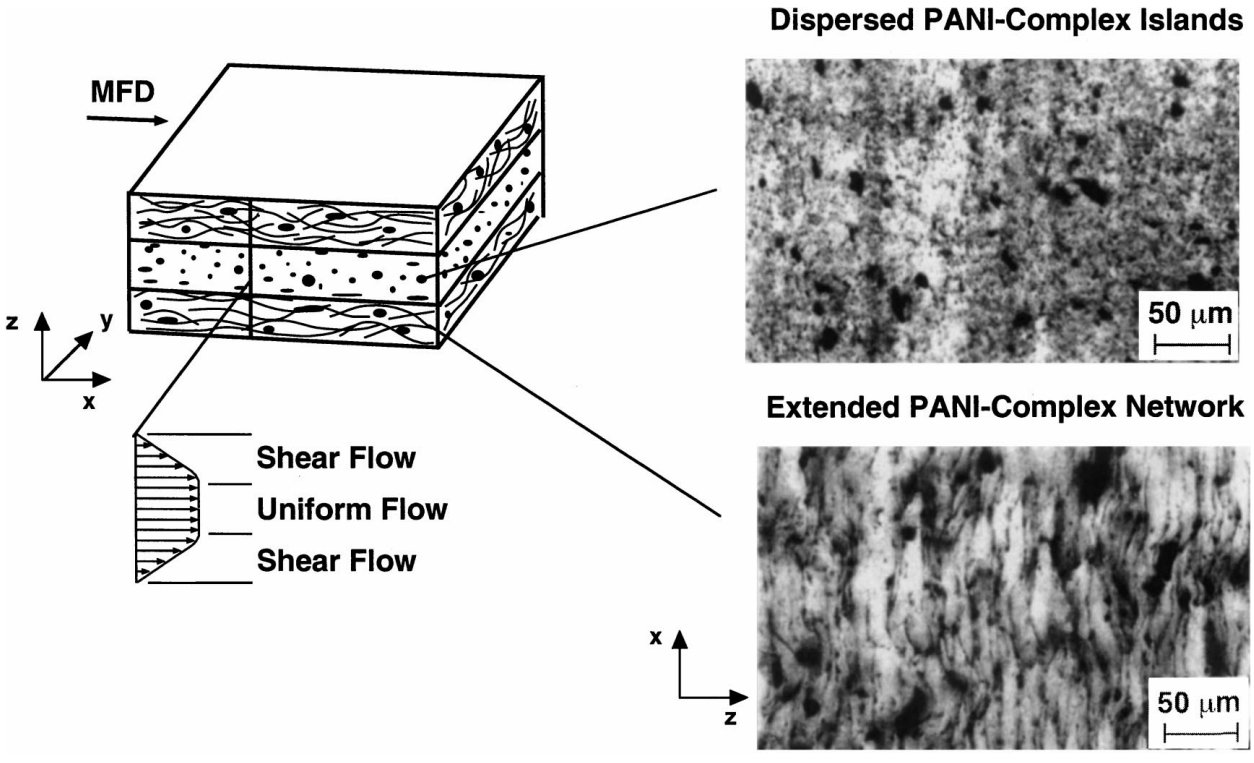

(b)

Figure 28 Production of gradient structures in particulate filled polymer systems: (a) schematic production processes; (b) gradient structure of an electrically conductive PANI-complex filled PP and (c) gradient in electrical conductivity over the cross section [44]. (*Continued*).

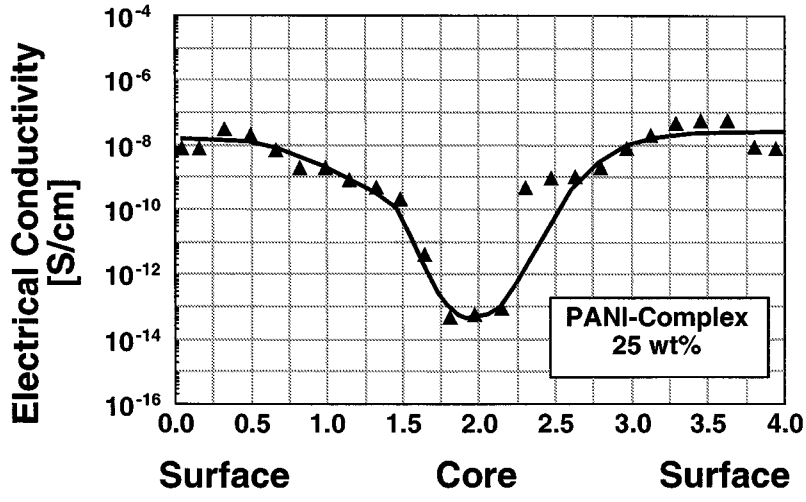

(c)

Figure 28 (*Continued*).

Acknowledgements

The author is grateful to the Fonds der Chemischen Industrie, Frankfurt, for support of his personal research activities in 1998. Further thanks are due to the Deutsche Forschungsgemeinschaft (DFG FR 675/7-2, 11-2 and 20-1). The critical pre-review of this article by Professor Robert C. Wetherhold, University of Buffalo, USA, and the courtesy of some text passages on hierarchical composite structures by R. F. Eduljee and R. L. McCullough, CCM, Delaware, USA, are also greatly esteemed. Part of the work was presented at a one day conference on "Mesoscopic Materials" at the University of Kyoto, Japan, in November 1997.

References

1. T. W. CHOU (ed.), "Structure and Properties of Composites," Vol. 13, edited by R. W. Cahn, P. Haasen, E. J. Kramer, *Materials Science and Technology* (VCH Publishers, Weinheim, Germany, 1993).
2. R. F. EDULJEE and R. L. McCULLOUGH, "Elastic Properties of Composites," *ibid*. p. 381.
3. M. R. PIGGOTT, *Comp. Sci. Technol.* **53**(2) (1995) 121.
4. S. W. YURGARTIS, *ibid.* 145.
5. M. HOJO, S. MATSUDA and S. OCHIAI, in Proc. ECCM-7, Seventh European Conf. on Composite Materials, London, May 14–16, 1996 (Woodhead Publishing, 1996) p. 81.
6. A. V. SRINIVASAN, G. K. HARITOS and F. L. HEDBERG, *Appl. Mech. Rev.* **44**(11) (1991) 463.
7. M. NOGUCHI and K. TAKAHASHI, Status and Prospects for Metal Matrix Composites in Japan, CMMC '96, Key Engineering Materials Vols. 127–131 (1997) p. 153.
8. K. FRIEDRICH, *Progr. Colloid Polym. Sci.* **66** (1979) 299.
9. K. FRIEDRICH, *ibid.* **64** (1978) 103.
10. K. FRIEDRICH, in "Crazing in Polymers, Advances in Polymer Science" edited by H. H. Kausch, Vol. 52/53 (Springer-Verlag, Berlin, 1983) p. 225.
11. E. HORNBOGEN, *Zeitschrift für Metallkunde* **68** (1977) 455.
12. K. FRIEDRICH, *Kunststoffe-German Plastics* **69** (1979) 796–801.
13. J. KARGER-KOCSIS, in "Application of Fracture Mechanics to Composite Materials," Composite Materials Series, Vol. 6, series edited by R. B. PIPES (Elsevier, Amsterdam, 1989) Chap. 6, pp. 189–247.
14. W. HELLERICH, G. HARSCH and S. HAENLE, Werkstoff-Führer Kunststoffe, Carl Hanser Verlag, München, Germany, 1989.
15. A. F. YEE and R. A. PEARSON, in "Fractography and Failure Mechanisms of Polymers and Composites" edited by A. C. Roulin-Moloney (Elsevier Appl. Sci., London, 1989) p. 291.
16. A. J. KINLOCH, in "Rubber Toughened Plastics," Adv. Chem. Ser. 222 edited by C. K. Riew (Am. Chem. Soc., Washington, 1989) p. 67.
17. J. KARGER-KOCSIS and K. FRIEDRICH, *Colloid Polym. Sci.* **270** (1992) 549.
18. J. F. HWANG, J. A. MANSON, R. W. HERTZBERG, G. A. MILLER and L. H. SPERLING, *Polym. Eng. Sci.* **29** (1989) 1477.
19. R. A. PEARSON and A. F. YEE, *J. Mater. Sci.* **26** (1991) 3828.
20. K. FRIEDRICH, *Plastics and Rubbers Processing and Applications* **3** (1983) 255.
21. R. C. WETHERHOLD, W. A. DICK and R. B. PIPES, SAE Technical Paper, No. 800812, 1980.
22. K. FRIEDRICH, *Comp. Sci. Technol.* **22** (1985) 43.
23. D. E. SPAHR, K. FRIEDRICH, R. S. BAILEY and J. M. SCHULTZ, J. Mater. Sci. **25** (1990) 4427.
24. K. FRIEDRICH, K. SCHULTE, G. HORSTENKAMP and T. W. CHOU, *ibid.* **20** (1985) 3353.
25. H. RICHTER, Processing and Application of Carbon Fiber Reinforced Polymers (in German), VDI-Gesellschaft Kunststofftechnik, Düsseldorf, Germany, 1981, 243.
26. D. HULL, "Introduction to Composite Materials," (Cambridge University Press, Cambridge, U.K., 1981).
27. J. SCHUSTER and K. FRIEDRICH, *Comp. Sci. Technol.* **57** (1997) 405.
28. K. FRIEDRICH, in Polypropylene: An A-Z Reference, edited by J. Karger-Kocsis (Chapman and Hall, London, 1998) in press.
29. W. J. TOMLINSON and J. R. HOLLAND, *J. Mater. Sci. Lett.* **13** (1994) 675.
30. B. J. DEVLIN, M. D. WILLIAMS, J. A. QUINN and A. G. GIBSON, *Composites Manufacturing* **2**(3/4) (1991) 203.
31. J. BLAUROCK and W. MICHAELI, *Engineering Plastics* **9** (1996) 282.
32. B. T. ÅSTRÖM and R. B. PIPES, in Proc. 46th Annual Conference (Composites Institute, The Society of Plastics Industry, February 18–21, 1991) Session 4-A, pp. 1–9.
33. K. FRIEDRICH and G. BECHTOLD, in Polypropylene: An A-Z Reference, edited by J. Karger-Kocsis (Chapman and Hall, London, 1998) in press.
34. V. KERBIRIOU, Impregnation and Pultrusion of Thermoplastic Composite Profiles (in German), Fortschrittberichte VDI, VDI Verlag, Düsseldorf, Germany, Reihe 5, Nr. 496, 1997.
35. V. KLINKMÜLLER, M. K. UM, M. STEFFENS, K. FRIEDRICH and B.-S. KIM, *Appl. Comp. Mat.* **1** (1995) 351.
36. R. C. HARPER, *SAMPE Journal* **28**(3) (1992) 9.
37. M. OSTGATHE, U. BREUER, C. MAYER and M. NEITZEL, in Proc. ECCM-7, Seventh European Conference on Composite Materials, Vol. 1 (Woodhead Publishing Ltd., Cambridge, U.K., 1996) p. 195.
38. K. FRIEDRICH, M. HOU and J. KREBS, in "Composite Sheet Forming," Vol. 11, Composite Materials Series, edited by R. B. Pipes (Elsevier Science, Amsterdam, 1997) Chap. 4, p. 91.

39. K. FRIEDRICH and M. HOU, On stamp forming of curved and flexible geometry components from continuous glass fiber/polypropylene Composites, *Composites Part A* (1997), to be published.
40. J. KREBS, K. FRIEDRICH, R. CHRISTIE and D. BHATTACHARYYA, in Proc. 4th Int. Conf. on Flow Processes in Composite Materials (FPCM '96 Aberystwyth, U.K., September 9–11, 1996) Session 10.
41. J. KREBS, D. BHATTACHARYYA and K. FRIEDRICH, *Composites Part A* **28** (1997) 481.
42. T. HARMIA and K. FRIEDRICH, *J. Theoretical and Applied Fracture Mechanics* **26** (1997) 47–52.
43. K. FRIEDRICH, in Proc. 5th Japan International SAMPE Symposium and Exhibition, (JISSE-5, Tokyo, Japan, October 28–31, 1997).
44. N. J. LEE, J. JANG, M. PARK and C. R. CHOE, *J. Mater. Sci.* **32** (1997) 2013.
45. M. FUNABASHI, in Proc. 5th Japan International SAMPE Symposium, October 28–31 (1997) pp. 187–192.
46. R. TAIPALUS, T. HARMIA and K. FRIEDRICH, *Applied Comp. Mat.* (1999) accepted.
47. Q. YUAN, K. FRIEDRICH and J. KARGER-KOCSIS, *Plastics, Rubber and Composites-Processing and Application* **22** (1994) 29.
48. J. KARGER-KOCSIS, E. MOOS and D. E. MOUZAKIS, *ibid.* **26**(4) (1997) 178–183.
49. I. NAUNDORF and P. EYERER, in "Polypropylene: An A-Z Reference," edited by J. Karger-Kocsis (Chapman and Hall, London, 1998) in press.
50. M. EVSTATIEV, S. FAKIROV and K. FRIEDRICH, *Applied Comp. Mat.* **2** (1995) 93.

Received 18 February
and accepted 14 September 1998